Pyrimidine inhibitors synergize with nucleoside analogues to block SARS-CoV-2

https://doi.org/10.1038/s41586-022-04482-x

Received: 22 October 2021

Accepted: 26 January 2022

Published online: 7 February 2022

Check for updates

David C. Schultz[1]✉, Robert M. Johnson[2,8], Kasirajan Ayyanathan[3,8], Jesse Miller[3,8], Kanupriya Whig[1], Brinda Kamalia[1], Mark Dittmar[3], Stuart Weston[2], Holly L. Hammond[2], Carly Dillen[2], Jeremy Ardanuy[2], Louis Taylor[2], Jae Seung Lee[3], Minghua Li[3], Emily Lee[4], Clarissa Shoffler[5], Christopher Petucci[5], Samuel Constant[6], Marc Ferrer[4], Christoph A. Thaiss[7], Matthew B. Frieman[2]✉ & Sara Cherry[1,3,7]✉

The SARS-CoV-2 virus has infected more than 261 million people and has led to more than 5 million deaths in the past year and a half[1] (https://www.who.org/). Individuals with SARS-CoV-2 infection typically develop mild-to-severe flu-like symptoms, whereas infection of a subset of individuals leads to severe-to-fatal clinical outcomes[2]. Although vaccines have been rapidly developed to combat SARS-CoV-2, there has been a dearth of antiviral therapeutics. There is an urgent need for therapeutics, which has been amplified by the emerging threats of variants that may evade vaccines. Large-scale efforts are underway to identify antiviral drugs. Here we screened approximately 18,000 drugs for antiviral activity using live virus infection in human respiratory cells and validated 122 drugs with antiviral activity and selectivity against SARS-CoV-2. Among these candidates are 16 nucleoside analogues, the largest category of clinically used antivirals. This included the antivirals remdesivir and molnupiravir, which have been approved for use in COVID-19. RNA viruses rely on a high supply of nucleoside triphosphates from the host to efficiently replicate, and we identified a panel of host nucleoside biosynthesis inhibitors as antiviral. Moreover, we found that combining pyrimidine biosynthesis inhibitors with antiviral nucleoside analogues synergistically inhibits SARS-CoV-2 infection in vitro and in vivo against emerging strains of SARS-CoV-2, suggesting a clinical path forward.

SARS-CoV-2 is a coronavirus, which is a family of single-stranded positive-sense RNA viruses, at least seven of which infect humans. RNA viruses including coronaviruses replicate using a virally encoded RNA-dependent RNA polymerase (RdRp), and nucleoside analogues, which are incorporated by the RdRp into the growing viral RNA chain, are a large class of approved direct-acting antivirals[3]. Depending on the analogue, incorporation can lead to chain termination or mutagenesis, ultimately inhibiting viral replication[4]. RdRps have conserved structures, and thus nucleoside analogues can show broad activity across related and unrelated viruses[5,6]. Therefore, repurposing efforts have identified nucleoside analogues that are active against newly emerging viruses, and such efforts have discovered that the nucleoside analogue remdesivir inhibits SARS-CoV-2 replication, becoming the first approved antiviral therapeutic against this novel coronavirus[7,8].

As all viruses, including SARS-CoV-2, are dependent on diverse cellular factors and metabolic products for their replication, the identification of host-directed antivirals also shows promise. In particular, host nucleoside biogenesis is required for viral replication as RNA viruses require high levels of nucleoside triphosphates for their growth. Widespread efforts are underway to identify essential host pathways that are druggable, and to repurpose therapeutics against these host targets. Respiratory epithelial cells are the major cellular target for SARS-CoV-2 in vivo. We and others have found that the cellular entry pathway as well as other host-dependent steps in the viral lifecycle show cell-type-specific differences and we were most interested in those antivirals that would be active in the respiratory tract[9]. Therefore, we used the human respiratory cell line Calu-3 for these studies. We set out to screen small-molecule libraries that contained approved drugs, drugs in clinical trials and drugs with known targets to uncover both direct-acting and host-directed antivirals using the ancestral SARS-CoV-2 virus (WA1) and a cell-based, high-content assay in respiratory cells. We optimized a microscopy-based assay to achieve robust screening parameters ($Z' > 0.5$) using vehicle (DMSO) and remdesivir (10 μM) as controls on each plate. We infected Calu-3 cells pre-treated with compounds and quantified infection of SARS-CoV-2 48 h after infection using an antibody to double-stranded RNA, a viral replication intermediate[9]. In addition, we quantified the number of cells in each well to remove drugs that were cytotoxic.

We screened approximately 18,000 drugs from three repurposing libraries: an in-house PENN library of approximately 3,500 drugs, about

[1]Department of Biochemistry and Biophysics, University of Pennsylvania, Philadelphia, PA, USA. [2]Department of Microbiology and Immunology, Center for Pathogen Research, University of Maryland School of Medicine, Baltimore, MD, USA. [3]Department of Pathology and Laboratory Medicine, University of Pennsylvania, Philadelphia, PA, USA. [4]National Center for Advancing Translational Sciences, National Institutes of Health, Rockville, MD, USA. [5]Metabolomics Core, Penn Cardiovascular Institute, University of Pennsylvania, Philadelphia, PA, USA. [6]Epithelix, Geneva, Switzerland. [7]Department of Microbiology, University of Pennsylvania, Philadelphia, PA, USA. [8]These authors contributed equally: Robert M. Johnson, Kasirajan Ayyanathan, Jesse Miller. ✉e-mail: dschultz@pennmedicine.upenn.edu; mfrieman@som.umaryland.edu; cherrys@pennmedicine.upenn.edu

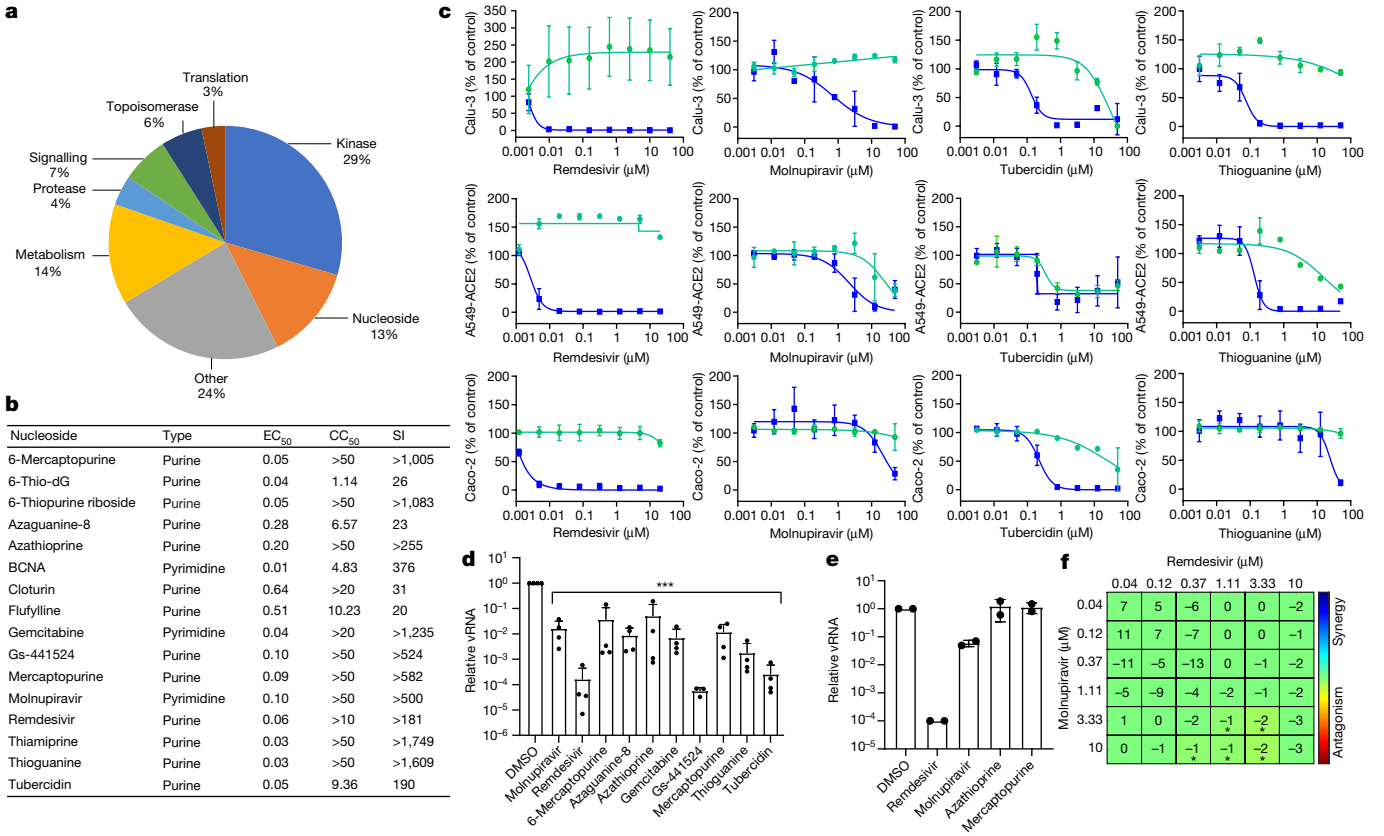

Nucleoside	Type	EC_{50}	CC_{50}	SI
6-Mercaptopurine	Purine	0.05	>50	>1,005
6-Thio-dG	Purine	0.04	1.14	26
6-Thiopurine riboside	Purine	0.05	>50	>1,083
Azaguanine-8	Purine	0.28	6.57	23
Azathioprine	Purine	0.20	>50	>255
BCNA	Pyrimidine	0.01	4.83	376
Cloturin	Purine	0.64	>20	31
Flufylline	Purine	0.51	10.23	20
Gemcitabine	Pyrimidine	0.04	>20	>1,235
Gs-441524	Purine	0.10	>50	>524
Mercaptopurine	Purine	0.09	>50	>582
Molnupiravir	Pyrimidine	0.10	>50	>500
Remdesivir	Purine	0.06	>10	>181
Thiamiprine	Purine	0.03	>50	>1,749
Thioguanine	Purine	0.03	>50	>1,609
Tubercidin	Purine	0.05	9.36	190

Fig. 1 | Antiviral nucleosides are highly active in respiratory cells and show cell-type-specific activity. a, Pie chart of antivirals validated in Calu-3 cells with selective index (EC_{50}/CC_{50}) > 3. From approximately 18,000 compounds, 122 show activity. **b**, Sixteen nucleoside analogues validated in Calu-3 cells with the nucleoside type listed along with the EC_{50}, CC_{50} and SI. **c**, Calu-3, A549-ACE2 or Caco-2 cells were treated with the indicated nucleosides in dose–response showing infection (blue) and toxicity (green). Data are presented as mean ± s.d. ($n = 3$ independent biological replicates). BCNA, bicyclic nucleoside analogue. **d**, Calu-3 cells pretreated with vehicle or 10 μM of the indicated drugs and infected with SARS-CoV-2 for 48 h and total RNA was subject to RT–qPCR analysis of viral infection. Data are presented as mean ± s.e.m. for reduction compared to vehicle control ($n = 4$ independent biological replicates) (***$P < 0.001$, one-way ANOVA; values are listed in Extended Data Fig. 1f). vRNA, viral RNA. **e**, RT–qPCR analysis of viral infection for the indicated drugs (remdesivir (10 μM), molnupiravir (10 μM), azathioprine (30 μM) and mercaptopurine (30 μM)) in nasal ALI cultures. Data are presented as mean ± s.e.m. ($n = 2$ independent biological replicates). **f**, BLISS analysis of the 2 × 2 combination of remdesivir and EIDD-2801 in Calu-3 cells showing additivity. Data are presented as mean values of excess over BLISS for $n = 9$ independent biological replicates. The statistical significance was determined by a one-sample Student's t-test (*$P < 5 \times 10^{-2}$).

3,400 drugs from the NCATS repurposing collection chosen to avoid overlap with the PENN library, and the ReFrame collection of roughly 11,300 drugs, most of which have been tested in humans[10]. Together, we screened a large fraction of the drugs that can potentially be rapidly repurposed, complementing previous screening efforts[9,11,12]. We screened the PENN library in duplicate at 0.8 μM and identified 77 drugs that inhibited infection by more than 60% and that had little toxicity (more than 80% cell viability) in each screen; the NCATS library at 0.8 μM and identified 45 drugs that inhibited infection by more than 60% and had little toxicity (more than 80% cell viability); and the ReFrame library in duplicate at 3.6 μM and identified 135 compounds that inhibited infection by more than 60% and had low toxicity (more than 60% cell viability) in both replicates (Extended Data Fig. 1a–c). We validated the candidates by repurchasing powders (PENN and NCATS) or testing pre-spotted validation plates (ReFrame) followed by in-house-created dose–response studies. This allowed us to determine potency (half maximal effective concentrations (EC_{50}s)) and toxicity (half maximal cytotoxic concentrations (CC_{50}s)) of each compound and focus on the 122 non-redundant compounds that had a selective index (SI) greater than 3 in Calu-3 cells (Fig. 1a, Supplementary Table 1 (and 102 drugs had a SI > 10)). These 122 compounds fall into a number of general categories, with nucleoside analogues accounting for 13% of the validated candidates.

Nucleoside analogues are a common class of drugs that are synthetic analogues that mimic their physiological counterparts and can be incorporated by cellular polymerases into DNA or RNA to inhibit cell division[4,13]. In addition, these can act as antimetabolites that deplete the supply of deoxynucleotides needed for DNA replication or nucleotides for RNA synthesis through inhibition of nucleoside biosynthesis enzymes[4]. Nucleoside analogues and antimetabolites are generally used to treat cancer and for immunosuppression. A subgroup of nucleoside analogues are direct-acting antivirals as they are incorporated specifically by viral polymerases, leading to defects in viral nucleic acid replication. Additional nucleoside analogues have been shown to have antiviral activity, probably through their antimetabolite activity; they are not incorporated but rather compete with cellular enzymes for their natural ligands. Two direct-acting antiviral nucleosides have been shown to block SARS-CoV-2 infection in vitro and in animal models and have been approved for use in humans[7,14]. Remdesivir is an adenosine analogue incorporated by the viral RdRp leading to delayed chain termination[15,16]. Molnupiravir (also known as EIDD-2801) is a cytosine analogue incorporated by the viral RdRp leading to increased viral mutagenesis and antiviral activity[14,17,18]. We identified remdesivir, the active metabolite of remdesivir, Gs-441524, and molnupiravir as antiviral in our unbiased screens (Fig. 1a, b). We identified 13 additional nucleoside analogues with antiviral properties

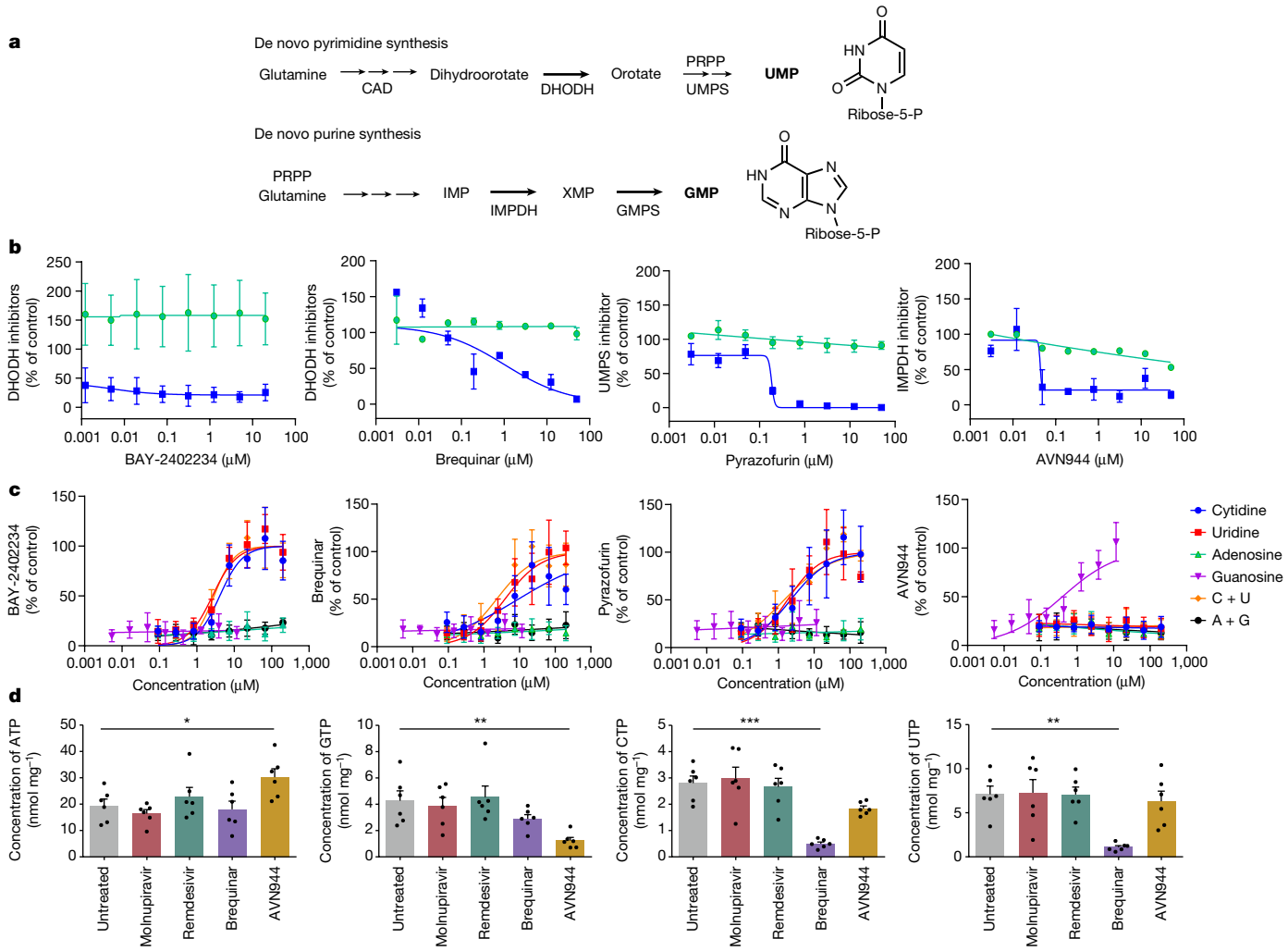

Fig. 2 | Inhibitors of host nucleoside metabolism are antiviral. a, Simplified schematic of nucleoside metabolism. Number of arrows indicates single versus multiple steps. CAD, carbamoyl-phosphate synthetase 2, aspartate transcarbamylase and dihydroorotase; GMPS, guanosine monophosphate synthetase; PRPP, phosphoribosyl diphosphate synthase. **b**, Dose–response analysis of the pyrimidine biosynthesis or purine biosynthesis inhibitors in Calu-3 cells. Infection (blue) and toxicity (green) are shown. Data are presented as mean ± s.d. ($n = 3$ independent biological replicates). **c**, Analysis of Calu-3 cells treated with the indicated inhibitor in the presence of increasing concentrations of the indicated nucleosides. Data are presented as mean ± s.d. ($n = 3$ independent biological replicates) for per cent infection. **d**, Calu-3 cells treated with the indicated inhibitor for 24 h and cell pellets subjected to liquid chromatography–mass spectrometry to quantify the nucleoside triphosphate levels. Mean ± s.e.m. is shown ($n = 6$ independent biological replicates). $^{*}P < 0.05$, $^{**}P < 0.01$, $^{***}P < 0.001$, one-way analysis of variance (ANOVA) with Dunnett's multiple comparisons test ($P = 0.0177$ (ATP) $P = 0.0045$ (GTP) $P < 0.0001$ (CTP) and $P = 0.0009$ (UTP)).

against SARS-CoV-2 (Fig. 1b, Extended Data Fig. 2). To determine the breadth of antiviral activity of the nucleosides, we tested a panel of cell lines that are permissive to infection with SARS-CoV-2, including human respiratory A549-expressing human ACE2, human intestinal epithelial Caco-2 cells, human hepatocyte Huh7.5 cells and African green monkey Vero cells (Fig. 1c, Extended Data Fig. 1d). The known direct-acting antivirals remdesivir and molnupiravir show activity across diverse cell types, with variable EC_{50}s (Fig. 1a–c, Extended Data Fig. 1d). We also found that the active form of molnupiravir, EIDD-1931, was active across cell types (Extended Data Fig. 3a). We also validated the antiviral activity of remdesivir and molnupiravir in Calu-3 cells using a quantitative reverse-transcription PCR (RT–qPCR) assay and found that these nucleoside analogues had strong antiviral activity by this orthogonal assay (Fig. 1d).

Some of the additional antiviral nucleoside analogues that we identified are thought to act as antimetabolites by competing with the natural ligands that inhibit enzymatic function and are generally used for cancer or immunosuppression[4] (for example, 6-mercaptopurine; Extended Data Fig. 1e). We found that these drugs are non-toxic in Calu-3 cells at the antiviral concentrations (Fig. 1a–c, Extended Data Fig. 1d, e), at least in part because these cells divide slowly. Moreover, we found that these antiviral nucleoside analogues show very divergent cell-type-specific activity and toxicities (Fig. 1a–d, Extended Data Fig. 1d, e). For example, tubercidin displays antiviral activity in Calu-3, Caco-2 and Huh7.5 cells with toxicity in A549-ACE2 and Vero cells. By contrast, thioguanine and 6-mercaptopurine are active in Calu-3 and A549-ACE2 cells but are not active in Caco-2 or Vero cells. We also monitored the antiviral activity of a subset of these nucleoside analogues in Calu-3 cells by RT–qPCR, and found that they all had significant antiviral activity (Fig. 1d). We also tested a subset of these antiviral nucleosides in primary human nasal air–liquid interface (ALI) cultures and found that only remdesivir and molnupiravir showed potent antiviral activity as measured by RT–qPCR (Fig. 1e). These studies demonstrated cell-type-specific antiviral activities of nucleoside analogues.

Given that the two direct-acting antiviral nucleosides are distinct nucleoside derivatives, with remdesivir, an adenosine analogue, and

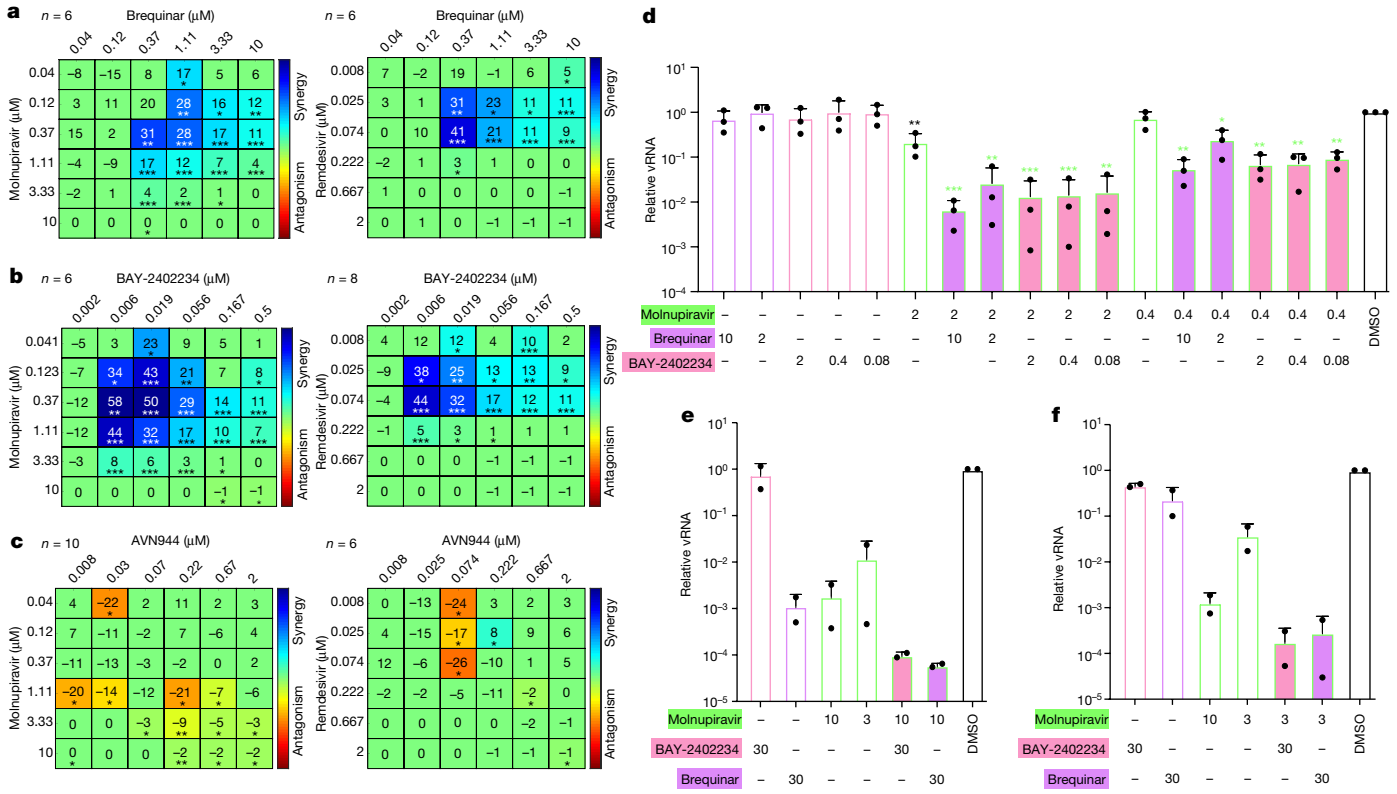

Fig. 3 | Combination of molnupiravir or remdesivir with DHODH inhibitors is synergistically antiviral in vitro. a–**c**, BLISS analysis in Calu-3 cells with molnupiravir or remdesivir in combination with the DHODH inhibitors Brequinar (**a**) or BAY-2402234 (**b**) and the IMPDH inhibitor AVN944 (**c**). Data are presented as mean values of excess over BLISS. The number of independent biological replicates (*n*) is indicated for the combination tested. Statistical significance was determined by a one-sample Student's *t*-test (*$P < 5 \times 10^{-2}$, **$P < 10^{-3}$ and ***$P < 10^{-4}$). **d**, Calu-3 cells were treated with the indicated drugs and infected with SARS-CoV-2. Total RNA was subject to RT–qPCR 48 h after infection for analysis of infection. Data are presented as mean ± s.e.m. for reduction compared to vehicle control ($n = 3$ independent biological replicates). The black asterisks show the *P* value relative to vehicle: **$P < 0.01$, using one-way ANOVA. The green asterisks show *P* values relative to single treatment with molnupiravir: *$P < 0.05$, **$P < 0.01$ and ***$P < 0.001$, using one-way ANOVA. *P* values are listed in Extended Data Fig. 8b. **e**, **f**, ALI-bronchial (**e**) or ALI-nasal (**f**) cells were treated with the indicated drugs and infected with SARS-CoV-2. Viral replication was quantified by RT–qPCR 72 h after infection and expression (vRNA/18S) was normalized to vehicle-treated cells. Data are presented as mean ± s.e.m. ($n = 2$ independent biological replicates). In **d**–**f**, the indicated drug concentration is in μM.

molnupiravir, a cytosine analogue, we tested whether the combination of these nucleosides would show antiviral synergy. Synergy is defined as having greater than an additive effect. Calu-3 cells were treated with six concentrations of each drug individually and in combination with each other, resulting in a matrix of 36 drug–x drug–y concentration pairs monitoring viral infection. We used BLISS analysis to determine whether the two drugs interact[19]. The null hypothesis in this model is that the drugs are additive, with a positive interaction leading to synergy and a negative interaction leading to antagonism. We found that the co-treatment of Calu-3 cells with remdesivir and molnupiravir during SARS-CoV-2 infection was additive (Fig. 1f, Extended Data Fig. 3b–d).

Antimetabolites are thought to act, at least in part, through inhibition of nucleoside biosynthesis by binding to metabolic enzymes and competing with the natural ligands[4]. Cells have two pathways for nucleoside biogenesis, de novo synthesis and salvage pathways that recycle purines and pyrimidines from degradation products. Although salvage pathways sustain cell viability, they cannot supply sufficient amounts of nucleoside triphosphates to allow for fast proliferation or support viral replication[20]. Therefore, in addition to applications in cancer, the inhibition of the de novo nucleotide biosynthesis constitutes a broad-spectrum antiviral strategy. In support of this, our screen identified a subset of known inhibitors of host-encoded nucleoside biosynthetic enzymes within the pyrimidine and purine biosynthetic pathways shown in Fig. 2a. This included three pyrimidine biosynthesis inhibitors: the two dihydroorotate dehydrogenase (DHODH) inhibitors BAY-2402234 and Brequinar, as well as the uridine monophosphate synthase (UMPS) inhibitor pyrazofurin. Dose–response studies showed that these drugs were active in Calu-3 cells with low toxicity (Fig. 2b). We did not identify the classical IMP dehydrogenase (IMPDH) inhibitors ribavirin or mycophenolic acid in our screens, although ribavirin and mycophenolic acid did inhibit viral infection at higher doses in Calu-3 cells (Extended Data Fig. 4a). We also tested the human respiratory cells A549-ACE2 and the panel of human cell lines that are permissive to SARS-CoV-2, and found that the DHODH inhibitors were active, whereas pyrazofurin had modest activity and AVN944 showed toxicity (Extended Data Fig. 4b, c).

We confirmed that the antiviral activity of the pyrimidine biosynthesis inhibitors was through nucleoside metabolism as we could fully block the antiviral activity of BAY-2402234, Brequinar or pyrazofurin by treating Calu-3 cells with the pyrimidine nucleosides cytidine and/or uridine, but not the purine nucleosides adenosine or guanosine (Fig. 2c). IMPDH is required for de novo guanosine biosynthesis, and thus treatment of cells with the purine guanosine, but not adenosine or the pyrimidine nucleosides, could reverse the antiviral activity of AVN944 (Fig. 2c). In addition, we monitored nucleoside pools upon treatment with the direct-acting nucleoside analogues remdesivir and molnupiravir and observed no changes in triphosphate levels of the four nucleotides (Fig. 2d). By contrast, treatment with the DHODH inhibitor Brequinar reduced levels of the pyrimidine triphosphates, whereas treatment with IMPDH inhibitor AVN944 reduced the levels

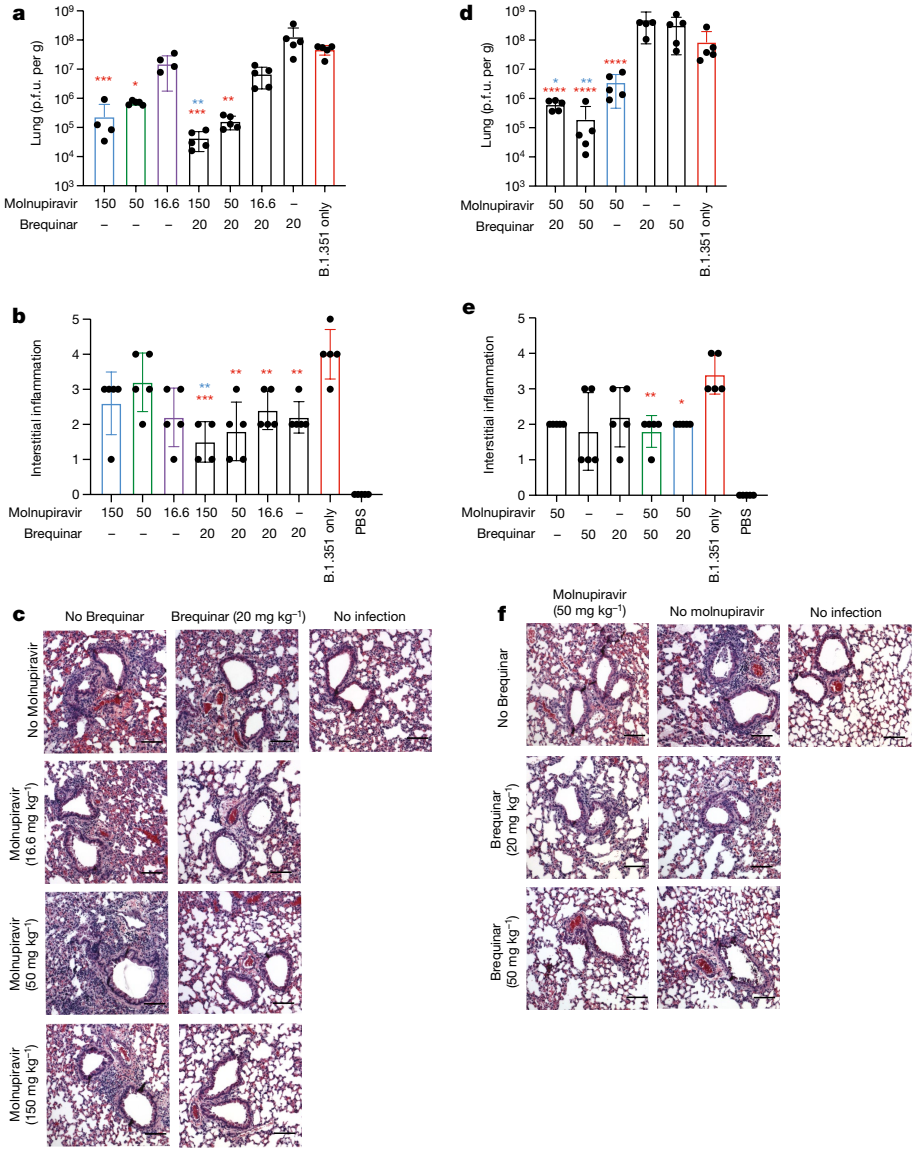

Fig. 4 | Combination of molnupiravir and Brequinar reduces SARS-CoV-2 infection and inflammation in vivo. Wild-type BALB/C mice were treated with Brequinar (intraperitoneal administration) and/or molnupiravir (oral administration) daily at the indicated concentrations starting 12 h before infection. Mice ($n = 5$ per group over 2 independent experiments) were intranasally inoculated with 1×10^5 p.f.u. per mouse of SARS-CoV-2 (B.1.351). **a**–**f**, Lungs were analysed for viral titre 2 days after infection by plaque assay (**a**, **d**) or fixed in 4% paraformaldehyde for haematoxylin and eosin staining and quantified for interstitial inflammation (**b**, **c**, **e**, **f**). $n = 5$ mice per group. Mean ± s.d. is shown. $^*P < 0.05$, $^{**}P < 0.01$ and $^{***}P < 0.001$, using non-parametric one-way ANOVA with Dunnett's multiple comparison test. The red asterisks are compared to vehicle; the blue asterisks are compared to molnupiravir. *P* values are listed in Extended Data Fig. 8d. Scale bars, 200 μM.

of guanosine triphosphates with increases in the production of ATP, which is produced from a common precursor that is shunted into that pathway upon inhibition of IMPDH (Fig. 2d). These data demonstrate that altering nucleoside pools can block viral replication in the absence of cytotoxicity.

Next, we set out to determine whether altering pyrimidine or purine pools using host-directed metabolic inhibitors would synergize with the antiviral nucleoside analogues remdesivir or molnupiravir. Using our microscopy-based assay, we performed 2 × 2 dose–response analysis. We found notable synergy between DHODH inhibitors (Brequinar or BAY-2402234) and nucleoside analogues (molnupiravir or remdesivir) (Fig. 3a, b, Extended Data Fig. 5). This synergy was observed in the submicromolar range of the DHODH inhibitor Brequinar and the low nanomolar range for BAY-2402234. We also tested whether the combination of molnupiravir or remdesivir with pyrazofurin, which inhibits UMPS, also shows synergy and found that it does (Extended Data Fig. 6a). By contrast, we observed little interaction between the IMPDH inhibitor AVN944 and either of the antiviral nucleoside analogues, with a modest trend towards antagonism (Fig. 3c, Extended Data Fig. 6b–d).

Given the emergence of SARS-CoV-2 variants and the promise of antivirals to have activity against diverse strains of SARS-CoV-2, we also tested whether these drugs were active against SARS-CoV-2 variants (Alpha, Beta, Gamma and Delta) and found that all strains were sensitive to molnupiravir, remdesivir and the pyrimidine biosynthesis inhibitors (Extended Data Fig. 7a). The ancestral strain (WA1) and Delta strain were also sensitive to AVN944, whereas the others were not. We focused on molnupiravir as it is an orally bioavailable drug and thus can be potentially used in an outpatient setting and is currently undergoing approvals[21,22]. We tested whether the combination of molnupiravir and the DHODH inhibitors would show antiviral synergy against SARS-CoV-2 variants. We observed synergy between

both DHODH inhibitors (Brequinar or BAY-2402234) and molnupiravir (Extended Data Fig. 7b). This suggests that limiting the pyrimidine pool in combination with the nucleoside analogue molnupiravir increases the antiviral activity of nucleoside analogues against diverse strains of SARS-CoV-2. The mechanism of this synergy is unclear; however, it may be due to increased uptake or incorporation of the nucleoside analogues when pyrimidines are limiting.

We further explored the activity and interactions between DHODH inhibitors and molnupiravir. We used an orthogonal assay to confirm that molnupiravir shows dose-dependent inhibition in Calu-3 cells using RT–qPCR (Fig. 3d, Extended Data Fig. 8a). As single agents, Brequinar and BAY-2402234 showed modest levels of inhibition as measured by RT–qPCR (Fig. 3d). However, when we combined treatments, we observed notable decreases in viral replication upon co-administration of either of these DHODH inhibitors and molnupiravir (Fig. 3d).

We next tested the activity of these inhibitors in air-liquid interface (ALI) respiratory epithelial cell cultures that more closely model the human respiratory epithelium. We used both tracheobronchial and nasal ALI cultures as these represent the two major sites of SARS-CoV-2 infection[23]. We performed additional studies to identify doses of these drugs that did not impact epithelial barrier function (by monitoring trans-epithelial electrical resistance), cilia beating frequency or toxicity (measuring lactate dehydrogenase release) in our nasal ALI cultures[24]. We found that treatment with molnupiravir, Brequinar or BAY-2402234 at concentrations up to 30 μM were non-toxic in this system (Extended Data Fig. 8c). Therefore, we used these doses as the maximum in our ALI cultures. In bronchial ALI cultures, we found that molnupiravir showed dose-dependent activity and that Brequinar had significant single-agent activity, whereas BAY-2402234 had little activity as a single agent in these cells (Fig. 3e). However, we found a significant reduction in viral replication upon co-treatment with either Brequinar or BAY-2402234 with molnupiravir (Fig. 3e). In the nasal cells, we found that molnupiravir showed dose-dependent activity and that neither Brequinar nor BAY-2402234 had significant single-agent activity (Fig. 3f). Again, we found a significant reduction in viral replication upon co-treatment of molnupiravir with either DHODH inhibitor (Fig. 3f).

Molnupiravir and Brequinar are both orally dosed drugs and molnupiravir has been approved in patients with COVID-19. We observed synergistic antiviral activity with this combination of drugs in diverse model cell systems; therefore, we set out to test whether this combination would also show benefit in the treatment of SARS-CoV-2 infection in vivo. We used a mouse model of infection in which wild-type BALB/C mice were intranasally inoculated with the SARS-CoV-2 Beta strain B.1.351 (1×10^5 plaque-forming units (p.f.u.) per mouse). In this model, we found robust replication 2 days after infection as measured by viral titres in the lungs (approximately 10^8 p.f.u per gram lung), bronchiolar sloughing of infected epithelial cells, and significant inflammatory cell infiltration including oedema with peribronchiolar and perivascular cuffing as measured by histology (Fig. 4). As expected, when we treated the animals with molnupiravir (EIDD-2801), we observed dose-dependent reduction in viral titres (Fig. 4a). In addition, there was only minor mitigation of the lung pathology with significant epithelial cell infection and inflammatory cell infiltration other than at the highest dose of molnupiravir tested (150 mg ml^{-1}) (Fig. 4b, c). We also treated mice with Brequinar alone, at doses similar to COVID-19 clinical trials (NCT04575038), and observed no effect on viral titres or lung pathology at 2 days after infection (Fig. 4a–c). Next, we combined treatments with multiple dosing of molnupiravir and a single dose of Brequinar (20mg kg^{-1}). We found an approximately 4 log reduction in viral titres upon co-treatment with Brequinar and molnupiravir at the highest dose of molnupiravir, and a significant reduction in titres at both 150 mg kg^{-1} and 50 mg kg^{-1} molnupiravir when combined with Brequinar compared with molnupiravir alone (Fig. 4a). We observed strong suppression of inflammation in the lung where, even at the lowest combination dose, there was reduced peribronchiolar and perivascular cuffing with lessened alveolar and interstitial inflammation and oedema (Fig. 4b, c). Moreover, co-treatment led to a clear protection of lung architecture with little alterations to bronchiolar and alveolar cells. These low doses of Brequinar are outside the toxic range and show protection. We also performed an experiment in which we used a single dose of molnupiravir (50 mg kg^{-1}) alone, and in combination with increasing doses of Brequinar (20 mg kg^{-1} and 50 mg kg^{-1}) (Fig. 4d–f). We again observed significant decreases in viral titres upon co-treatment of molnupiravir and Brequinar over molnupiravir alone (Fig. 4d). Histological analysis revealed that treatment with molnupiravir modestly reduced SARS-CoV-2-induced pathology and that co-administration with Brequinar further reduced the inflammatory response seen with molnupiravir alone (Fig. 4b, c, e, f).

We also performed a study using therapeutic dosing in this model. We infected mice intranasally, and on day 1 after infection, we treated infected mice with molnupiravir, Brequinar or the combination and quantified viral infection and inflammation in the lungs on day 3 after infection. We found that the addition of Brequinar to molnupiravir reduced viral titres and inflammation (Extended Data Fig. 9). Together, this combination of molnupiravir and Brequinar for COVID-19 treatment shows promise as we observed both reduction in viral replication and decreased pathology when dosed before or after infection.

Given that for many viral infections combinations of antivirals are needed to suppress infection, we suggest that combining nucleoside analogues with DHODH inhibitors would be beneficial, as the combination would both reduce replication and inflammation due to SARS-CoV-2 infection within therapeutic ranges. Owing to the recent success of the SARS-CoV-2 protease inhibitor Paxlovid (Pfizer; PF-07321332), we also tested the combination of this drug with molnupiravir or remdesivir against SARS-CoV-2 Beta or Delta strains. We found that these combinations are additive (Extended Data Fig. 10). Thus, there are numerous potential combinations that should be tested in clinical trials that may alter the trajectory of the current pandemic.

Online content

Any methods, additional references, Nature Research reporting summaries, source data, extended data, supplementary information, acknowledgements, peer review information; details of author contributions and competing interests; and statements of data and code availability are available at https://doi.org/10.1038/s41586-022-04482-x.

1. Lu, R. et al. Genomic characterisation and epidemiology of 2019 novel coronavirus: implications for virus origins and receptor binding. *Lancet* **395**, 565–574 (2020).
2. Huang, C. et al. Clinical features of patients infected with 2019 novel coronavirus in Wuhan, China. *Lancet* **395**, 497–506 (2020).
3. Huchting, J. Targeting viral genome synthesis as broad-spectrum approach against RNA virus infections. *Antivir. Chem. Chemother.* **28**, 2040206620976786 (2020).
4. Jordheim, L. P., Durantel, D., Zoulim, F. & Dumontet, C. Advances in the development of nucleoside and nucleotide analogues for cancer and viral diseases. *Nat. Rev. Drug Discov.* **12**, 447–464 (2013).
5. Sheahan, T. P. et al. Comparative therapeutic efficacy of remdesivir and combination lopinavir, ritonavir, and interferon beta against MERS-CoV. *Nat. Commun.* **11**, 222 (2020).
6. Agostini, M. L. et al. Coronavirus susceptibility to the antiviral remdesivir (GS-5734) is mediated by the viral polymerase and the proofreading exoribonuclease. *mBio* **9**, e00221-18 (2018).
7. Pruijssers, A. J. et al. Remdesivir inhibits SARS-CoV-2 in human lung cells and chimeric SARS-CoV expressing the SARS-CoV-2 RNA polymerase in mice. *Cell Rep.* **32**, 107940 (2020).
8. Sheahan, T. P. et al. Broad-spectrum antiviral GS-5734 inhibits both epidemic and zoonotic coronaviruses. *Sci. Transl. Med.* **9**, eaal3653 (2017).
9. Dittmar, M. et al. Drug repurposing screens reveal cell-type-specific entry pathways and FDA-approved drugs active against SARS-Cov-2. *Cell Rep.* **35**, 108959 (2021).
10. Janes, J. et al. The ReFRAME library as a comprehensive drug repurposing library and its application to the treatment of cryptosporidiosis. *Proc. Natl Acad. Sci. USA* **115**, 10750–10755 (2018).
11. Bakowski, M. A. et al. Drug repurposing screens identify chemical entities for the development of COVID-19 interventions. *Nat. Commun.* **12**, 3309 (2021).
12. Riva, L. et al. Discovery of SARS-CoV-2 antiviral drugs through large-scale compound repurposing. *Nature* **586**, 113–119 (2020).

13. Yates, M. K. & Seley-Radtke, K. L. The evolution of antiviral nucleoside analogues: a review for chemists and non-chemists. Part II: complex modifications to the nucleoside scaffold. *Antiviral Res.* **162**, 5–21 (2019).
14. Sheahan, T. P. et al. An orally bioavailable broad-spectrum antiviral inhibits SARS-CoV-2 in human airway epithelial cell cultures and multiple coronaviruses in mice. *Sci. Transl. Med.* **12**, eabb5883 (2020).
15. Jordan, P. C. et al. Initiation, extension, and termination of RNA synthesis by a paramyxovirus polymerase. *PLoS Pathog.* **14**, e1006889 (2018).
16. Tchesnokov, E. P., Feng, J. Y., Porter, D. P. & Gotte, M. Mechanism of inhibition of Ebola virus RNA-dependent RNA polymerase by remdesivir. *Viruses* **11**, 326 (2019).
17. Agostini, M. L. et al. Small-molecule antiviral β-D-N^4-hydroxycytidine inhibits a proofreading-intact coronavirus with a high genetic barrier to resistance. *J. Virol.* **93**, e01348-19 (2019).
18. Urakova, N. et al. β-D-N^4-hydroxycytidine is a potent anti-alphavirus compound that induces a high level of mutations in the viral genome. *J. Virol.* **92**, e01965-17 (2018).
19. Ma, J. & Motsinger-Reif, A. Current methods for quantifying drug synergism. *Proteom. Bioinform.* **1**, 43–48 (2019).
20. Ariav, Y., Ch'ng, J. H., Christofk, H. R., Ron-Harel, N. & Erez, A. Targeting nucleotide metabolism as the nexus of viral infections, cancer, and the immune response. *Sci. Adv.* **7**, eabg6165 (2021).
21. Wahl, A. et al. SARS-CoV-2 infection is effectively treated and prevented by EIDD-2801. *Nature* **591**, 451–457 (2021).
22. Cox, R. M., Wolf, J. D. & Plemper, R. K. Therapeutically administered ribonucleoside analogue MK-4482/EIDD-2801 blocks SARS-CoV-2 transmission in ferrets. *Nat. Microbiol.* **6**, 11–18 (2021).
23. Hou, Y. J. et al. SARS-CoV-2 reverse genetics reveals a variable infection gradient in the respiratory tract. *Cell* **182**, 429–446.e14 (2020).
24. Pizzorno, A. et al. Characterization and treatment of SARS-CoV-2 in nasal and bronchial human airway epithelia. *Cell Rep. Med.* **1**, 100059 (2020).

Methods

Viruses and cells

SARS-CoV-2 WA1 was provided by the BEI/CDC. SARS-CoV-2 (Alpha, Beta, Gamma and Delta) was provided by A. Pekosz (Johns Hopkins University School of Public Health). Virus stocks were amplified using the ARTIC primer set[25] and sequenced using the MinION system (Oxford Nanopore Technologies) by the J. Craig Venter Institute (MD, USA) to more than 4,000× genome coverage. Stock sequence was verified by aligning reads to the reference genome provided by the BEI (GSAID accession: EPI_ISL_890360) using minimap2 version 2.22 with the 'map-ont' presets[26], followed by inspection of the consensus sequence and alignment using IGV[27]. Stocks had less than 1% variation. Stock virus was prepared by infection of Vero E6 cells expressing TMPRSS2 in growth medium (DMEM (Quality Biological), supplemented with 10% (v/v) fetal bovine serum (Gibco), 1% (v/v) penicillin–streptomycin (Gemini Bio-products) and 1% (v/v) L-glutamine (2 mM final concentration; Gibco) fetal bovine serum plus for 2 or 3 days when cytopathic effect (CPE) was visible. Media were collected and clarified by centrifugation before being aliquoted for storage at −80 °C. Titre of stock was determined by plaque assay or 50% tissue culture infectious dose ($TCID_{50}$) analysis using Vero E6 cells as previously described[5]. All work with infectious virus was performed in a biosafety level 3 laboratory and approved by the University of Pennsylvania Biosafety Committee and the University of Maryland School of Medicine Institutional Biosafety Committee.

Vero cells (American Type Culture Collection (ATCC), CCL81 or E6) and Huh7.5 cells (C. Rice, Rockefeller) were cultured in DMEM, supplemented with 10% (v/v) fetal bovine serum, 1% (v/v) penicillin–streptomycin and 1% (v/v) L-Glutamax (Invitrogen). Calu-3 cells (ATCC, HTB-55) were cultured in MEM, supplemented with 10% (v/v) fetal bovine serum, 1% (v/v) penicillin–streptomycin, 1% (v/v) L-glutamine and 1% (v/v) non-essential amino acids. A549-ACE2 cells were cultured in RPMI1640 supplemented with 10% (v/v) fetal bovine serum, 1% (v/v) penicillin–streptomycin and 1% (v/v) L-Glutamax. Caco-2 cells (ATCC, HTB-37) were cultured in MEM alpha supplemented with 20% (v/v) fetal bovine serum, 1% (v/v) penicillin–streptomycin and 1% (v/v) L-glutamine. All cells were grown at 37 °C, 5% CO_2 and 20% O_2. All cell lines were validated by morphology and gene expression and are mycoplasma free.

Day 20 air–liquid interface (ALI) EpiAirway tracheobronchial tissues were obtained from MatTek (AIR-100) and used after day 30. Tissues were fed twice a week until use. ALI-pooled nasal epithelial cultures from Epithelix were fed twice a week until use. Toxicity studies were performed on nasal air–liquid interface cultures. Daily basolateral exposure of test compounds was evaluated using tissue integrity (trans-epithelial electrical resistance (TEER)); cytotoxicity was measured as basolateral lactate dehydrogenase (LDH) release and cilia beating frequency at 72 h.

Tissue integrity (TEER). Tissue integrity was determined by monitoring TEER using the EVOM3 Ohm Meter (World Precision Instruments). Resistance values (Ω) were converted to TEER (Ω cm^2) using the following formula: TEER (Ω cm^2) = (resistance value (Ω) − 100(Ω)) × 0.33 (cm^2), where 100 Ω is the resistance of the membrane and 0.33 cm^2 is the total surface of the epithelium.

Cytotoxicity (LDH release). Basolateral LDH release was quantified using Cytotoxicity LDH Assay Kit-WST (Dojindo, CK12–20), measuring the absorbance of each sample at 490 nm with a microplate reader. To determine the percentage of cytotoxicity, the following equation was used (A = absorbance values): cytotoxicity (%) = (A (exp value) − A (low control)/A (high control) − A (low control)) × 100. The high-control value was obtained by 10% Triton X-100 apical treatment (24 h). Triton X-100 causes a massive LDH release and corresponds to 100% cytotoxicity.

Cilia beating frequency. Cilia beating frequency was measured using the following setup: a Sony XCD V60 camera connected to an Olympus BX51 microscope with a ×5 objective and a camera-specific software. The cilia beating frequency is expressed as Hz. 256 images were captured at a high-frequency rate (125 frames per second) at 34 °C. Cilia beating frequency was then calculated using Cilia-X software (Epithelix).

High-throughput screening

Ten-thousand Calu-3 cells were plated per well of 384-well assay plates (Corning) in 20 µl of growth medium. For the PENN and NCATS libraries, 50 nl of drugs was added at a final concentration of 0.8 µM in 0.2% DMSO. For the ReFrame library, 20 µl of MEM was dispensed to compound source plates pre-spotted with 50 nl of 10 mM compound in DMSO. Of diluted compound, 5 µl was added per well of 384-well assay plate, yielding a final concentration of 3.6 µM in 0.04% DMSO. The positive control, 10 µM remdesivir (n = 32), and the negative control, 0.2% DMSO (n = 32), were spotted on each plate. One hour after the addition of the drugs, cells were infected with SARS-CoV-2 (multiplicity of infection (MOI) = 0.5). Cells were fixed 40–48 h post-infection in 4% formaldehyde in PBS for 15 min at room temperature, washed three times with PBS, blocked with 2% BSA in PBST for 60 min, and incubated in primary antibody (anti-double-stranded RNA J2, absolute antibody, 1:500) overnight at 4 °C. Cells were washed three times in PBST with an automated plate washer (BioTek) and incubated in secondary antibody (anti-mouse Alexa 488, 1:1,000 and Hoescht 33342) for 1 h at room temperature. Cells were washed three times in PBST with an automated plate washer and imaged using an automated microscope (ImageXpress Micro, Molecular Devices). Cells were imaged with a ×10 objective, and four sites per well were captured. The total number of cells and the number of infected (double-stranded RNA^+) cells were measured using the cell scoring module (MetaXpress 5.3.3), and the percentage of infected cells was calculated. The aggregated percent infection of the 0.2% DMSO (n = 32) and 10 µM remdesivir control wells (n = 32) on each assay plate were used to calculate z'-factors, as a measure of assay performance and data quality. Sample well infection was normalized to aggregated DMSO plate control wells and expressed as percentage of control (POC = (%$infection_{sample}$/average %$infection_{DMSO}$) × 100) and Z score (Z = (%$infection_{sample}$ − average %$infection_{DMSO}$)/standard deviation %$infection_{DMSO}$) in Spotfire (PerkinElmer). Candidate hits were selected as the following: for the UPENN screen, compounds with POC < 40% for infection and viability > 80% in either replicate; for the NCATS screen, POC < 40% for infection and viability > 80%; for the ReFrame screen, POC < 50% for infection and > 60% viability for the average of the replicates, compared to DMSO control.

Dose–response studies

Candidate drugs from the UPENN and NCATS library were purchased as powders from Selleckchem, MedchemExpress, Cayman and MedKoo and suspended in DMSO. Drugs were arrayed in 8-pt dose–response in 384-well plates. For the ReFrame validation, 15 µl of MEM was dispensed to compound source plates pre-spotted with 100 nl of compound in DMSO arrayed in an 8-pt dose–response. Of the diluted compound, 5 µl was added per well of 384-well assay plate, yielding final concentrations of 9.5, 3.1, 1.0, 0.35, 0.12, 0.04, 0.01 and 0.004 µM in 0.1% DMSO. Calu-3 (n = 10,000), A549-ACE2 (n = 3,000), Caco-2 (n = 1,500), Huh7.5 (n = 3,000) or Vero (n = 3,000) cells were plated in 384-well plates. Twenty-four hours after plating (72 h for Caco-2), drug additions and infections were performed using the screening conditions. DMSO (0.2%; n = 32) and 10 µM remdesivir (n = 32) were included on each plate as controls for normalization. For nucleoside rescue experiments, cells were treated with an EC_{90} concentration of a given nucleoside biosynthesis inhibitor in combination with a dose–response of nucleosides. Infection at each drug concentration was normalized to aggregated DMSO

plate control wells and expressed as POC (POC = %infection$_{sample}$/average %infection$_{DMSO\ cont}$) × 100. A non-linear regression curve fit analysis (GraphPad Prism 8) was performed on POC of percent infection and cell viability using $\log_{10}$-transformed concentration values to calculate EC_{50} values for percent infection and CC_{50} values for cell viability for each drug–cell line combination. The EC_{50} and CC_{50} values represent the average of two or more independent experimental replicates. SI was calculated as a ratio of the CC_{50} and EC_{50} values ($SI = CC_{50}/EC_{50}$) of a drug.

Quantitative drug combination analysis

Using our high-throughput screening assay conditions, drugs were added to Calu-3 cells in 384-well assay plates using a Tecan D300e dispenser in a matrix that combined six concentrations of remdesivir (up to 2 μM) or molnupiravir (up to 10 μM) with six concentrations of Brequinar (up to 10 μM), BAY-2402234 (up to 0.5 μM) and AVN944 (up to 2 μM), resulting in 36 concentration combinations per drug pair in 0.2% DMSO. Each combination was independently repeated at least three times as technical duplicates in each biological replicate. Sample well infection was normalized to aggregated 0.2% DMSO plate control wells ($n = 32$) and expressed as POC. Synergy between drug combinations was determined by the BLISS independence model, to quantitatively assess drug interaction patterns within the drug–drug combination matrix .The BLISS expectation (E) for a combined response was calculated by $E = (A + B) - (A \times B)$ where A and B are the fractional inhibition of SARS-CoV-2 infection of drug A and drug B at a given dose. The difference between the BLISS expectation and the observed inhibition of SARS-CoV-2 infection for the combination of drug A and drug B at the same dose is the BLISS value. BLISS values between 0 and 10 indicate that the combination is additive (as expected for independent pathway effects); BLISS value > 20 indicates activity greater than additive (synergy); and BLISS value < 0 indicates the combination is less than additive (antagonism).

RT–qPCR

Calu-3 cells (750,000 cells per well) were plated in six-well plates. The next day, drugs were added to cells. One hour later, cells were infected with SARS-CoV-2 (MOI = 0.3). For ALI cultures, the apical surface was washed with OptiMEM, and cells were placed into fresh medium with drugs added to the basolateral surface. Cells were infected apically with SARS-CoV-2 (MOI = 0.2) for 1 hour and, subsequently, the virus inoculum was removed. The cells were placed into fresh medium daily with the indicated drugs. Total RNA was purified using TRIzol (Invitrogen) followed by the RNA Clean and Concentrate kit (Zymo Research) 48 h after infection for Calu-3 and 72 h after infection for ALI cultures. For cDNA synthesis, reverse transcription was performed with random hexamers and Moloney murine leukaemia virus (M-MLV) reverse transcriptase (Invitrogen). Synthesized RNA was used as a standard (BEI). Gene-specific primers to SARS-CoV-2 (Wuhan v1, NSP14) and SYBR green master mix (Applied Biosystems) were used to amplify viral RNA, and 18S rRNA primers were used to amplify cellular RNA using the QuantStudio 6 Flex RT–PCR system (Applied Biosystems). Relative quantities of viral and cellular RNA were calculated using the standard curve method[3]. Viral RNA was normalized to 18S RNA for each sample (Wuhan V1/18S)[4].

Metabolomics

Calu-3 cells treated for 24 h with the indicated drugs were snap-frozen in liquid nitrogen, and thawed cell pellets on ice were homogenized with ice-cold 80% methanol. The samples were vortexed for 10 s to lyse cells and the cell homogenate was spiked with isotopically labelled nucleotide internal standards. The mixture was extracted with ice-cold methanol, vortexed and centrifuged at 18,100*g* for 5 min at 4 °C. The supernatant was dried under nitrogen at 45 °C and reconstituted in 50% methanol for liquid chromatography–mass spectrometry on an Agilent 1290 Infinity UHPLC/6495B triple quadrupole mass spectrometer. A 12-min linear gradient from 95% B (acetonitrile) to 54% A (10 mM ammonium acetate, pH 9, and 0.1% medronic acid) on an Agilent PEEK HILIC-z 2 × 100 mm, 2.7-μm column was used to separate nucleotides. Multiple reaction monitoring was used to quantitate a fragment ion of the parent ion of each nucleotide with standard calibration curves. The raw data were normalized from μM to nmol mg^{-1} protein using a BCA assay from input samples.

Mouse studies

Mouse challenge studies were approved by the University of Maryland School of Medicine IACUC. Eight to ten-week-old female BALB/C mice were randomized and not blinded. Molnupiravir (#HY-135853, MedChemExpress) was resuspended in corn oil (8267, Sigma) and 10% DMSO (2438, Sigma), with dosing twice a day as oral gavage. Brequinar (#HY-108325, MedChemExpress) was resuspended in 10% DMSO and sterile saline, with dosing daily as intraperitoneal injection. Our pharmacokinetic (PK) studies showed an approximately 10 h half-life of Brequinar, and dosing was either started at 12 h before infection or 24 h after infection as indicated.

Mice were anaesthetized by intraperitoneal injection with 50 μl of a mix of xylazine (0.38 mg per mouse) and ketamine (1.3 mg per mouse) diluted in PBS. Mice were intranasally inoculated with 1×10^5 p.f.u. of the Beta variant of SARS-CoV-2 in 50 μl. Challenged mice were weighed on the day of infection and daily for 2 days after infection; there were no significant changes in weights observed. For prophylactic dosing, 2 days after infection, or therapeutic dosing 3 days after infection, five mice were killed from each treatment and control group, lungs were collected to determine viral titre by a plaque assay, and fixed in 4% paraformaldehyde for 24 h before sectioning and staining with haematoxylin and eosin by UMSOM Histology Core[5]. Pathological scoring on blinded haematoxylin and eosin-stained sections was performed for each mouse and analysed for inflammation.

Statistical analyses

Statistics were performed with GraphPad Prism 9.2 software. Lung titres for the treatment groups were compared to vehicle and statistically analysed using a non-parametric one-way ANOVA with Dunnett's multiple comparison test. For metabolomics, one-way ANOVA with Dunnett's post-hoc test for multiple comparisons was used to determine significance from vehicle control. For RT–qPCR, two-way ANOVA test was used. For the synergy studies, Combenefit software (update 1 June 2016) was used. Statistical methods were not used to predetermine sample size. Blinding and randomization were not used.

Reporting summary

Further information on research design is available in the Nature Research Reporting Summary linked to this paper.

Data availability

All data in this paper are presented in the main text and supplementary text. Supplementary Information is available for this paper. Source data are provided with this paper.

25. Tyson, J. R. et al. Improvements to the ARTIC multiplex PCR method for SARS-CoV-2 genome sequencing using nanopore. Preprint at bioRxiv https://doi.org/10.1101/2020.09.04.283077 (2020).
26. Li, H. Minimap2: pairwise alignment for nucleotide sequences. *Bioinformatics* **34**, 3094–3100 (2018).
27. Robinson, J. T. et al. Integrative genomics viewer. *Nat. Biotechnol.* **29**, 24–26 (2011).

Acknowledgements We thank members of the Cherry, Lynch, Frieman and Penn Center for Precision Medicine for advice and discussion; R. Perera for viral preparations; D. Nguyen for his data analysis and all members of the High-Throughput Screening Core at University of Pennsylvania for reagents and technical support; the Penn Metabolomics Core in the Cardiovascular Institute for liquid chromatography–mass spectrometry quantitation of nucleotides; S. Weiss and Y. Li for sharing SARS-related coronavirus 2, isolate USA-WA1/2020;

A. Pekosz for SARS-CoV-2 variants (Alpha, Beta, Gamma and Delta); X. Hu, R. Eastman, M. Hall and members of NCATS Compound Management for assembly and preparation of the NCATS compound collections; and CALIBR for providing the ReFrame library and validation plates. This work was supported by grants from the National Institutes of Health to S. Cherry (R01AI074951, R01AI122749, 1R21AI151882 and R01AI140539), as well as funding from the Penn Center for Precision Medicine, Mercatus and the Bill and Melinda Gates Foundation (INV-018479). S. Cherry is a recipient of the Burroughs Wellcome Investigators in the Pathogenesis of Infectious Disease Award, the Deans Innovation Fund as well as Linda and Laddy Montague. Work at the NCATS was funded by the by the Intramural Research Program of the National Center for Advancing Translational Sciences, National Institutes of Health (ZIA Project #TR000414-01). M.B.F., R.M.J., H.L.H. and S.W. are supported by funding from Bill and Melinda Gates Foundation (INV-016638), NIH R21AI158134, NIH R21AI153480 and HHS/BARDA ASPR-20-01495.

Author contributions D.C.S., R.M.J., E.L., S. Constant, M.F., M.B.F. and S. Cherry. conducted research design. D.C.S., R.M.J., K.A., J.M., K.W., B.K.,M.D., S.W., H.L.H., C.D., J.A., L.T., J.S.L., M.L., E.L., C.S., C.P., S. Constant, M.F., M.B.F. and S. Cherry. performed the experiments. D.C.S., R.M.J., K.A., J.M., K.W., B.K., M.D., S.W., H.L.H., C.D., J.S.L., M.L., E.L., C.P., S. Constant, M.F., M.B.F. and S. Cherry conducted the data analysis. D.C.S., E.L., S. Constant, M.F., C.A.T., M.B.F. and S. Cherry wrote the manuscript. D.C.S., S. Constant, M.F., M.B.F. and S. Cherry. supervised the study.

Competing interests The authors declare no competing interests.

Additional information

Supplementary information The online version contains supplementary material available at https://doi.org/10.1038/s41586-022-04482-x.

Correspondence and requests for materials should be addressed to David C. Schultz, Matthew B. Frieman or Sara Cherry.

Peer review information *Nature* thanks the anonymous reviewers for their contribution to the peer review of this work.

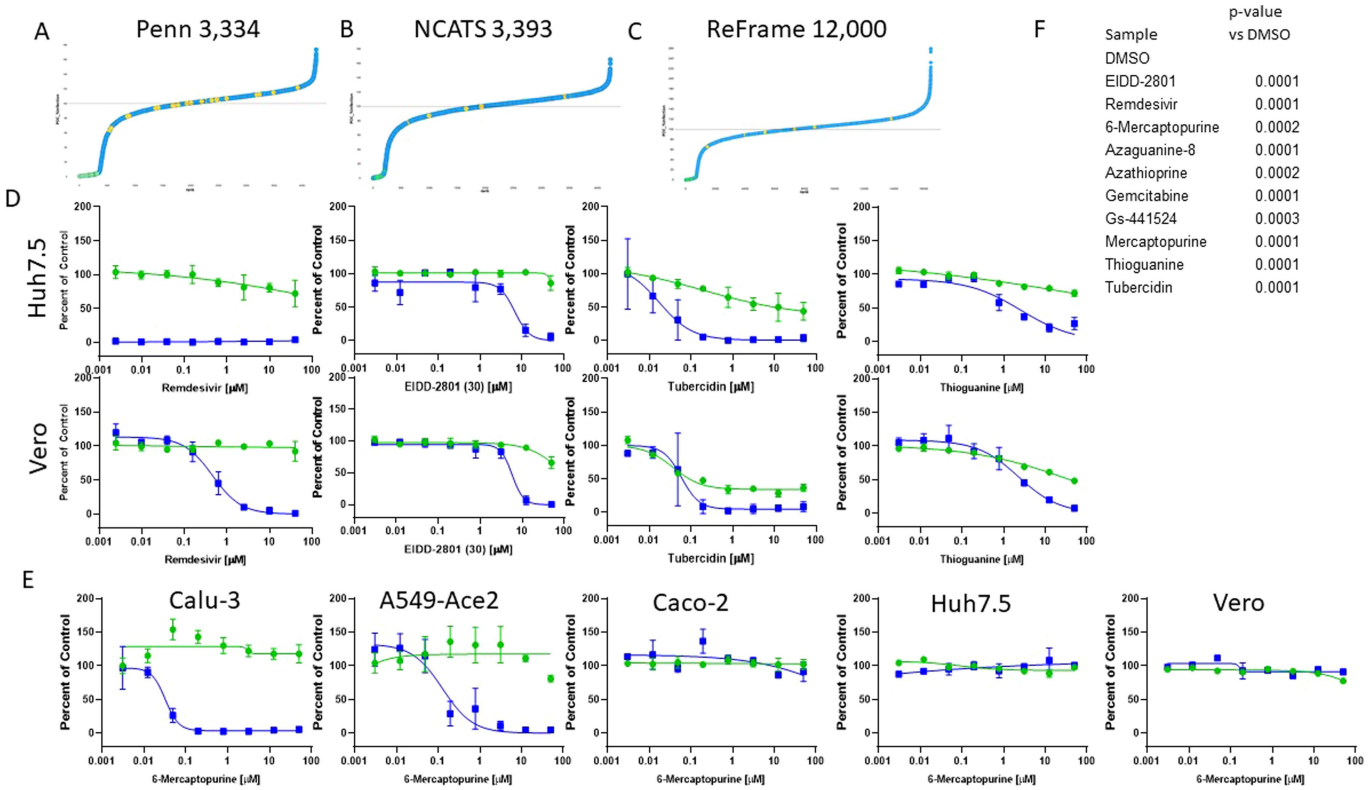

F

Sample	p-value vs DMSO
DMSO	
EIDD-2801	0.0001
Remdesivir	0.0001
6-Mercaptopurine	0.0002
Azaguanine-8	0.0001
Azathioprine	0.0002
Gemcitabine	0.0001
Gs-441524	0.0003
Mercaptopurine	0.0001
Thioguanine	0.0001
Tubercidin	0.0001

Extended Data Fig. 1 | High-throughput screening in Calu-3 cells to identify antivirals against SARS-CoV-2. a–**c**, High throughput screening of ~18,000 drugs including the (**a**) UPENN library, (**b**) NCATS library and (**c**) ReFrame library in Calu-3 cells infected with SARS-CoV-2. Percent of Control (POC) for % infection is plotted versus rank of the drug across the primary screens. Yellow circles, DMSO controls; Green circles, remdesivir controls; Blue Circles, sample wells. Solid horizontal line represents 100% Infection of DMSO control wells. **d**, Huh7.5 or Vero (CCL81) cells were treated with the indicated nucleosides in dose response showing infection (blue) and toxicity (green). Data are presented as mean ± SD (n = 3 independent biological replicates). **e**, The indicated cell line was treated with increasing doses of 6-mercaptopurine and dose responses for infection (blue) and toxicity (green) are shown. Data are presented as mean ± SD (n = 3 independent biological replicates). **f**, p-values from Fig. 1d.

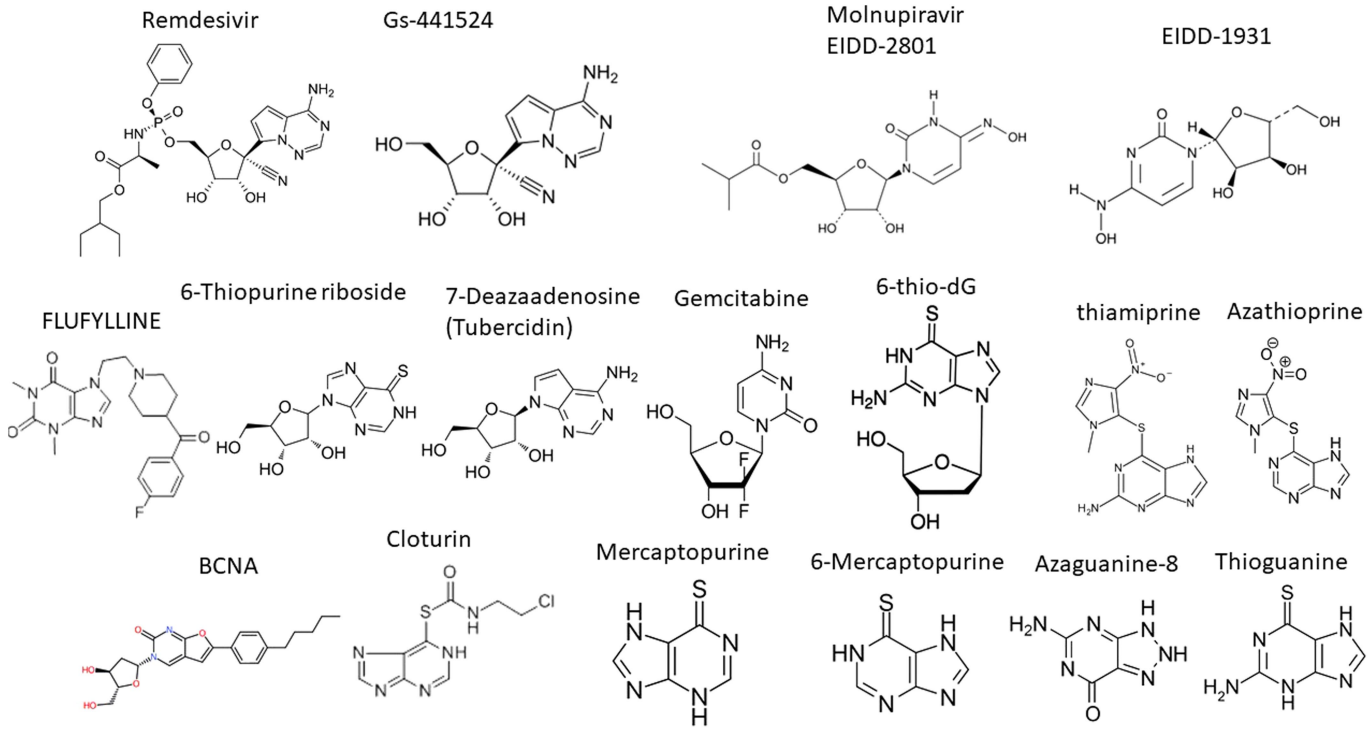

Extended Data Fig. 2 | Structures of antiviral nucleoside analogs shown. Nucleoside-related analog structures shown.

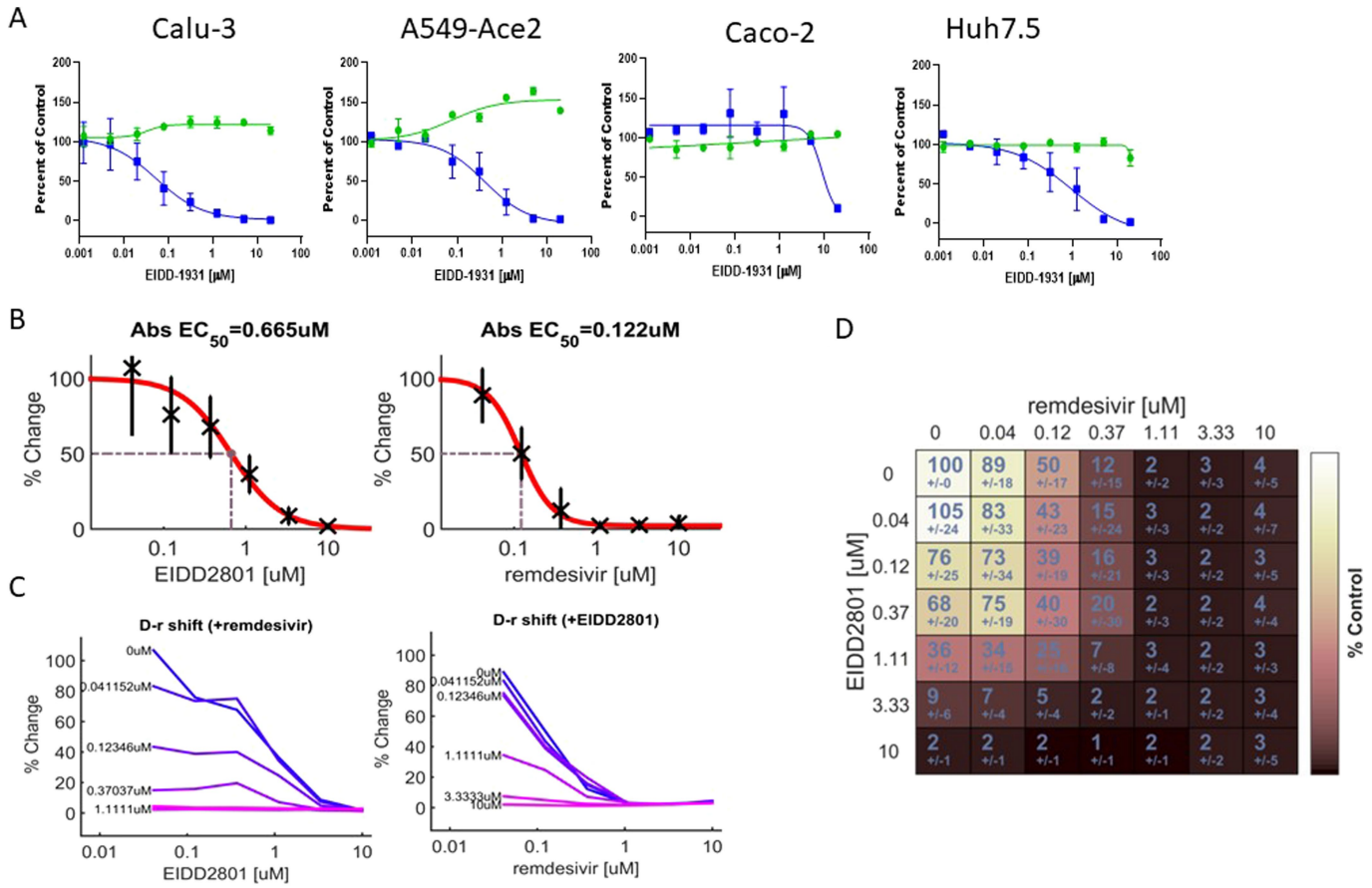

Extended Data Fig. 3 | Combination of remdesivir and molnupiravir is additive. a, The indicated cell line was treated with increasing doses of EIDD-1931 and dose responses for infection (blue) and toxicity (green) are shown. Data are presented as mean ± SD (n = 3 independent biological replicates). **b**, anti-SARS2 activity of remdesivir and molnupiravir as single agents. Data are presented as mean ± SD. **c**, anti-SARS2 activity of remdesivir in combination with a single concentration of molnupiravir or molnupiravir in combination with a single concentration of remdesivir. **d**, Two-dimensional representation of dose response interaction matrix for percent of control of infection mean ± SD, n = 9 independent biological replicates.

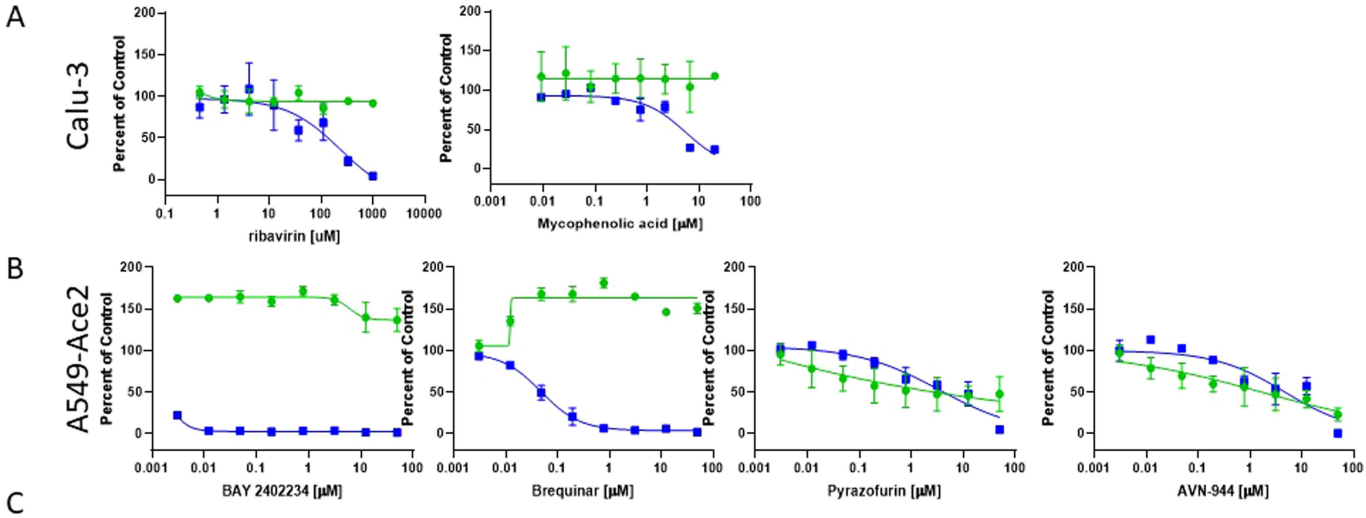

C

SARS-CoV-2 WA1	A549-ACE2			Caco-2			Huh7.5		
	EC50	CC50	SI	EC50	CC50	SI	EC50	CC50	SI
remdesivir	0.010	> 10	> 777	0.03	>4	>136	0.003	>4	>1271
molnupiravir	4.4	> 50	11	22.6	>50	>2	6.8	>50	>7
BAY-2402234	< 0.003	> 50	> 16667	>20	>20	1	0.001	>20	>20000
brequinar	0.0500	> 50	> 1043	>50	>50	1	0.5	>50	>983
AVN-944	4.75	1.7	1	39	>50	1	0.8	0.46	1

Extended Data Fig. 4 | Inhibitors of host nucleoside metabolism are antiviral. a, Calu-3 cells were treated with the indicated IMPDH inhibitors in dose response showing infection (blue) and toxicity (green). Data are presented as mean ± SD (n = 4 independent biological replicates). **b**, A549-Ace2 cells were treated with the indicated inhibitors in dose response showing infection (blue) and toxicity (green). Data are presented as mean ± SD (n = 4 independent biological replicates). **c**, Table of the EC50, CC50 and SI for the indicated cell line and drug (uM).

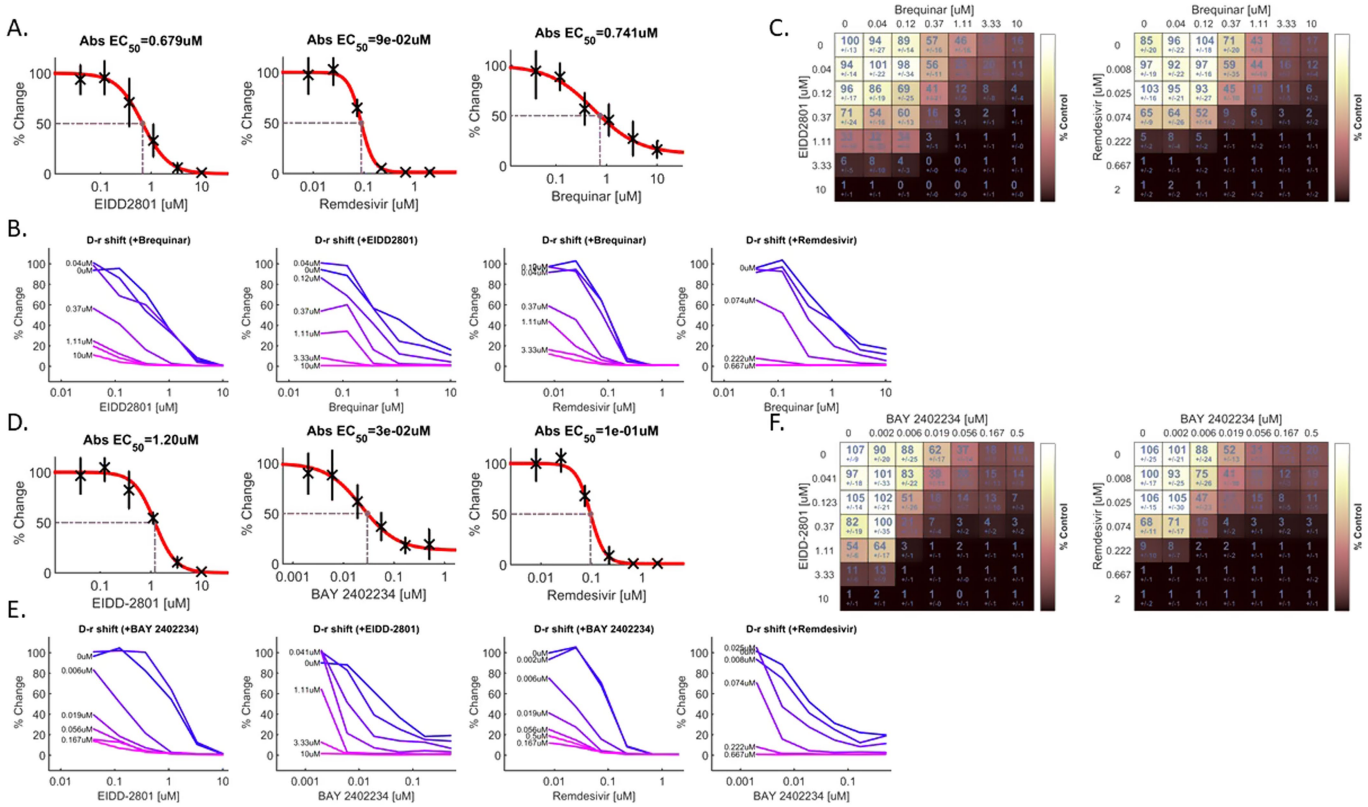

Extended Data Fig. 5 | Combination of molnupiravir or remdesivir with DHODH inhibitors are synergistically antiviral in vitro. a, Anti-SARS2 activity of molnupiravir, remdesivir, and Brequinar, as single agents. Data are presented as mean ± SD. **b**, Anti-SARS2 activity of molnupiravir or remdesivir in combination with a single concentration of Brequinar. **c**, Two-dimensional representation of dose response interaction matrix for percent of control of infection. Data are presented as mean ± SD (n = 6 independent biological replicates). **d**, Anti-SARS2 activity of molnupiravir, remdesivir, and BAY-2402234, as single agents. Data are presented as mean ± SD. **e**, Anti-SARS2 activity of molnupiravir or remdesivir in combination with a single concentration of BAY-2402234. **f**, Two-dimensional representation of dose response interaction matrix for percent of control of infection. Data are presented as mean ± SD (n = 6 for EIDD-2801, n = 8 for remdesivir for independent biological replicates).

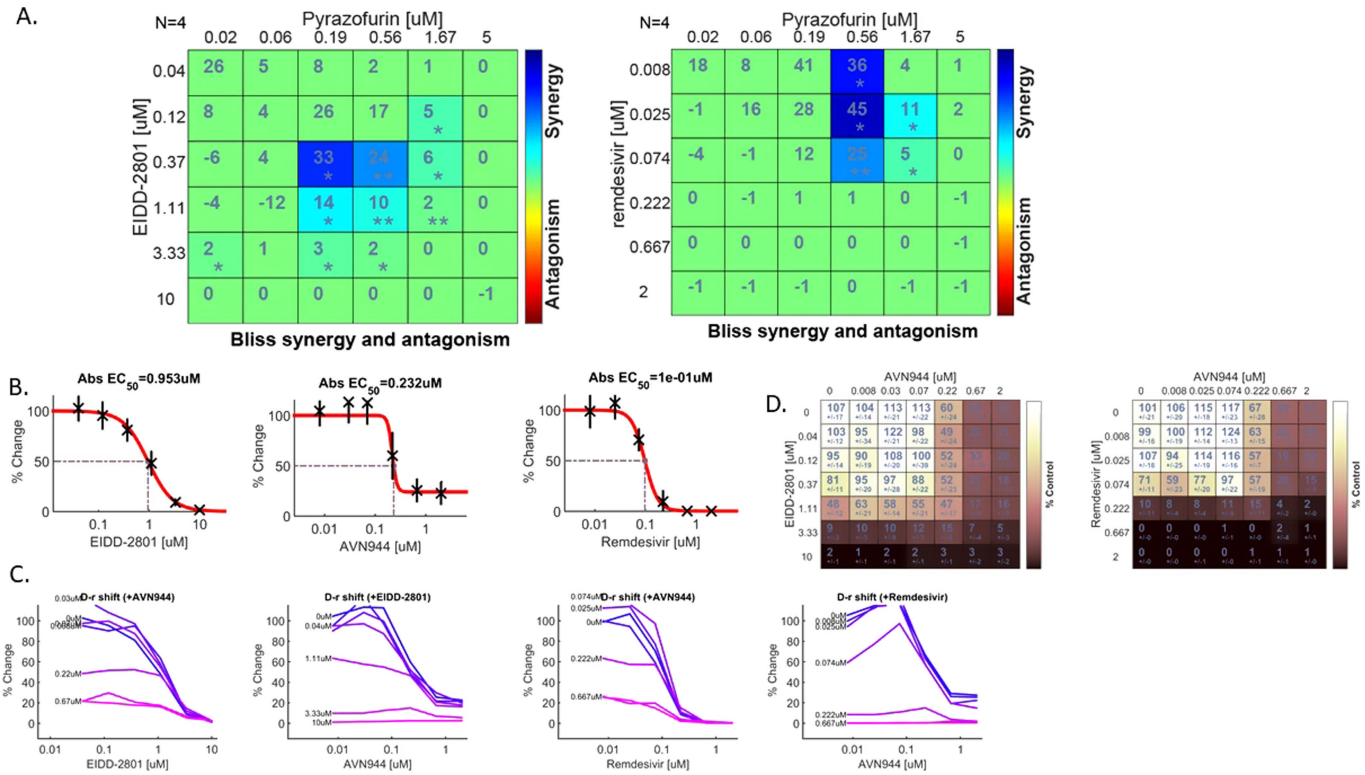

Extended Data Fig. 6 | Combination of molnupiravir or remdesivir with Pyrazofurin but not AVN944 is synergistically antiviral in vitro. a, BLISS analysis in Calu3 cells with molnupiravir (EIDD-2801) or remdesivir in combination with pyrazofurin. Data are presented as mean values of Excess over BLISS. (n = 4 independent biological replicates). The statistical significance was determined by a one-sample t-test (* $p < 5x10^{-2}$; ** $p < 10^{-3}$). **b**, Anti-SARS2 activity of molnupiravir, remdesivir, and AVN944 as single agents. Data are presented as mean ± SD. **c**, Anti-SARS2 activity of molnupiravir or remdesivir in combination with a single concentration of AVN944. **d**, Two-dimensional representation of dose response interaction matrix for percent of control of infection. Data are presented as mean ± SD (n = 10 for EIDD-2801, n = 6 for remdesivir for independent biological replicates).

A

	SARS-CoV-2 WA1			SARS-CoV-2 Alpha			SARS-CoV-2 Beta			SARS-CoV-2 Gamma			SARS-CoV-2 Delta		
	EC50	CC50	SI	EC50	CC50	SI	EC50	CC50	SI	EC50	CC50	SI	EC50	CC50	SI
remdesivir	0.123	>4	>32	0.051	>2	>40	0.049	>2	>41	0.101	>2	>20	0.079	>2	>25
molnupiravir	0.708	>50	>71	1.138	>10	>9	1.39	>10	>7	2.263	>10	>4	1.271	>10	>8
BAY-2402234	0.005	>20	>4000	0.006	>0.5	>83	0.009	>0.5	>56	0.011	>0.5	>50	0.006	>0.5	>83
brequinar	0.794	>50	>62	0.144	>10	>69	0.697	>10	>14	0.629	>10	>16	0.379	>10	>26
AVN-944	0.044	>50	>1141	5	>10	>2	>2	>2	1	>10	>10	1	0.271	>10	>37
pyrazofurin	0.185	>50	>270	0.775	>5	>6	0.466	>5	>11	0.602	>5	>8	0.377	>5	>13
PF-07321332	0.173	>5	>29	0.21	>2.5	>12	0.225	50	>222	0.282	>2.5	>9	0.203	>5	>25

B

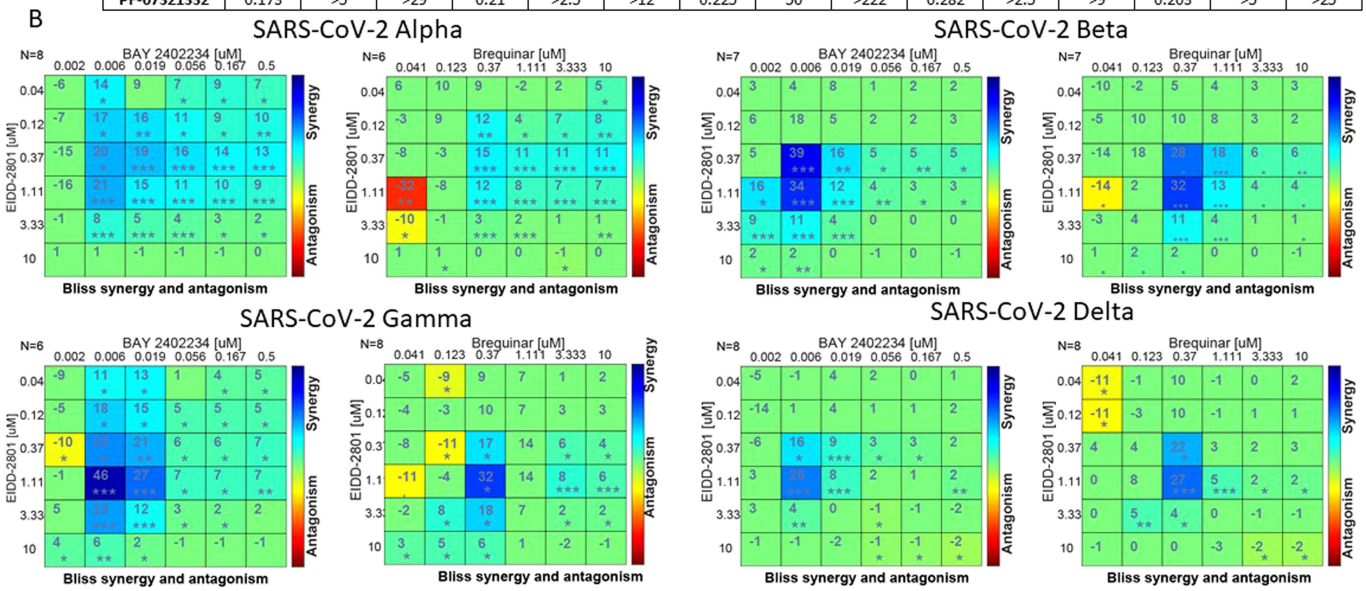

Extended Data Fig. 7 | Combination of molnupiravir with DHODH inhibitors is synergistic against SARS-CoV-2 variants. a, Table of EC50, CC50 and SI for the indicated variant and the indicated drugs (uM) in Calu-3 cells. **b**, BLISS analysis in Calu3 cells with molnupiravir (EIDD-2801) in combination with DHODH inhibitors Brequinar or BAY-2402234 infected with the indicated variant. Data are presented as mean values of Excess over BLISS. The following number of independent replicates were performed: SARS-CoV2 Alpha; n = 8 for BAY2402234, n = 6 Brequinar; SARS-CoV2 Beta; n = 7, SARS-CoV2 Gamma; n = 6 BAY2402234, n = 8; SARS-CoV2; Delta: n = 8. The statistical significance was determined by a one-sample t-test (* $p < 5x10^{-2}$; ** $p < 10^{-3}$, *** $p < 10^{-4}$).

A

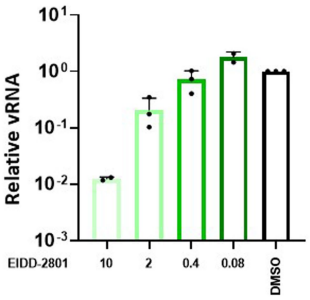

B

Sample	p-value vs DMSO	p-value vs 2uM EIDD-2801	p-value vs 0.4uM EIDD-2801
10.0μM Brequinar	0.1822		
2.0μM Brequinar	0.7706		
2.0μM BAY 2402234	0.2153		
0.4μM BAY 2402234	0.712		
0.08μM BAY 2402234	0.7315		
2.0μM EIDD-2801	0.006		
2.0μM EIDD-2801 + 10.0μM Brequinar		0.0007	
2.0μM EIDD-2801 + 2.0μM Brequinar		0.0015	
2.0μM EIDD-2801 + 2.0μM BAY 2402234		0.0009	
2.0μM EIDD-2801 + 0.4μM BAY 2402234		0.001	
2.0μM EIDD-2801 + 0.08μM BAY 2402234		0.001	
0.4μM EIDD-2801	0.4575		
0.4μM EIDD-2801 + 10.0μM Brequinar			0.0025
0.4μM EIDD-2801 + 2.0μM Brequinar			0.0138
0.4μM EIDD-2801 + 2.0μM BAY 2402234			0.0028
0.4μM EIDD-2801 + 0.4μM BAY 2402234			0.0033
0.4μM EIDD-2801 + 0.08μM BAY 2402234			0.004
DMSO			

Figure S8

C

Maximal tested tolerated dose in nasal air-liquid interface cultures at 72h post basolateral daily exposure

Compound	TEER	CBF	LDH
Molnupiravir	30 uM	30 uM	30 uM
Remdesivir	30 uM	30 uM	30 uM
Brequinar	30 uM	30 uM	30 uM
BAY2402234	30 uM	30 uM	30 uM
AVN944	30 uM	>10 uM	10 uM

D

	Summary	Adjusted P Value
Figure 4A		
(red stars)		
B.1.351 Only vs. EIDD-2801 (150 mg/kg)	***	0.0002
B.1.351 Only vs. EIDD-2801 (50 mg/kg)	*	0.0452
B.1.351 Only vs. EIDD (150 mg/kg) +Breq (20 mg/kg)	***	0.0002
B.1.351 Only vs. EIDD (50 mg/kg) +Breq (20 mg/kg)	**	0.0032
(blue stars)		
EIDD-2801 (150 mg/kg) vs. EIDD (150 mg/kg) +Breq (20 mg/kg)	**	0.0087
Figure 4B		
(red stars)		
B.1.351 Only vs. EIDD (150 mg/kg) +Breq (20 mg/kg)	***	0.0008
B.1.351 Only vs. EIDD (50 mg/kg) +Breq (20 mg/kg)	**	0.0071
B.1.351 Only vs. EIDD (16.6 mg/kg) +Breq (20 mg/kg)	**	0.0018
B.1.351 Only vs. Brequinar (20 mg/kg)	**	0.0029
(blue stars)		
EIDD-2801 (150 mg/kg) vs. EIDD (150 mg/kg) +Breq (20 mg/kg)	**	0.0031
Figure 4D		
(red stars)		
B.1.351 Only vs. EIDD (50 mg/kg) +Breq (20 mg/kg)	****	<0.0001
B.1.351 Only vs. EIDD (50 mg/kg) +Breq (50 mg/kg)	****	<0.0001
B.1.135 Only vs. EIDD-2801 (50 mg/kg)	****	<0.0001
(blue stars)		
EIDD-2801 (50 mg/kg) vs. EIDD (50 mg/kg) +Breq (20 mg/kg)	*	0.0122
EIDD-2801 (50 mg/kg) vs. EIDD (50 mg/kg) +Breq (50 mg/kg)	**	0.0021
Figure 4E		
(red stars)		
B.1.351 Only vs. EIDD (50 mg/kg) +Breq (50 mg/kg)	**	0.0059
B.1.351 Only vs. EIDD (50 mg/kg) +Breq (20 mg/kg)	*	0.021

Extended Data Fig. 8 | Nucleoside-related drugs are well-tolerated in air-liquid interface cultures. a, Calu-3 cells were treated with the indicated concentrations of Molnupiravir (EIDD-2801) and infected with SARS-CoV-2. 48hpi viral replication was quantified by RT-qPCR and expression (viral RNA/18S) was normalized to vehicle treated cells. Data are presented as mean±SEM for n = 2-3 biological replicates. **b**, P-values for Fig. 3d. **c**, Nasal air-liquid interface cells were treated daily on the basolateral side with the indicated concentrations of drug, and at 72 h TEER, Cilia beating frequency (CBF) and toxicity (LDH) were measured. **d**, P-values for Fig. 4.

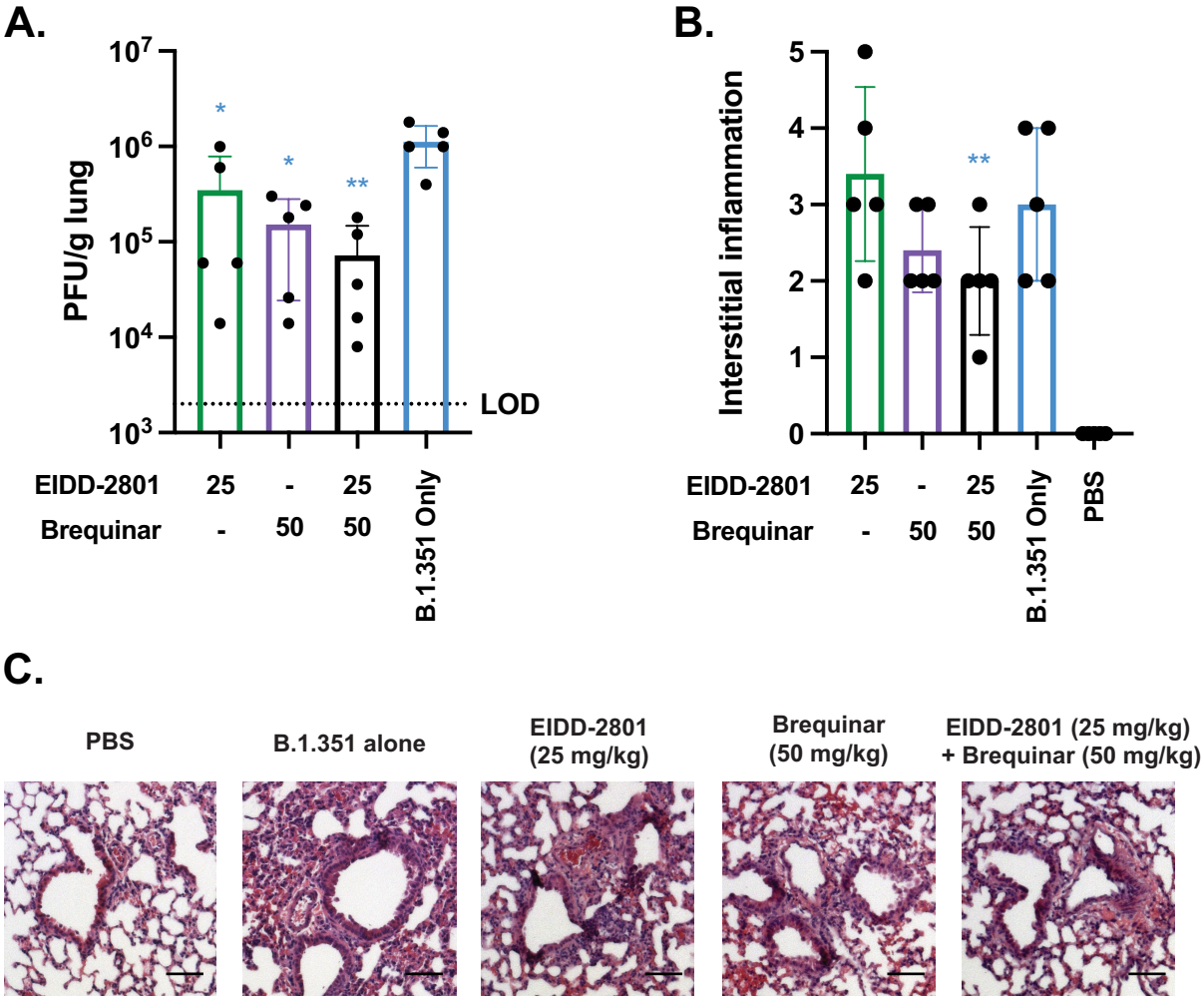

Extended Data Fig. 9 | Combination of molnupiravir and Brequinar reduces SARS-CoV-2 infection and inflammation in vivo during therapeutic dosing. Wild type Balb/C mice were treated with Brequinar (IP) and/or molnupiravir (EIDD-2801) (PO) daily at the indicated concentrations starting 24 h after infection. Mice (N = 5 mice per group) were intranasally inoculated with $1x10^5$ PFU/mouse of SARS-CoV-2/B.1.351. **a**, 3 dpi, lungs analyzed for viral titer by plaque assay, Mean±SD shown. * $p < 0.05$, ** $p < 0.01$, non-parametric one-way ANOVA with Dunnett's multiple comparison test. (p-values: B1.135 only vs EIDD-2801 (25 mg/kg) = 0.045, vs EIDD-2801 (50 mg/kg = 0.016, vs EIDD-2801 (25 mg/kg)+ Breq (50 mg/kg) = 0.0017. **b**, **c**, 3 dpi, lungs fixed in 4% PFA for H&E staining (Scale bar = 200 µM) and quantified for interstitial inflammation. Mean±SD shown. ** $p < 0.01$, non-parametric one-way ANOVA with Dunnett's multiple comparison test. (p-value = 0.0015).

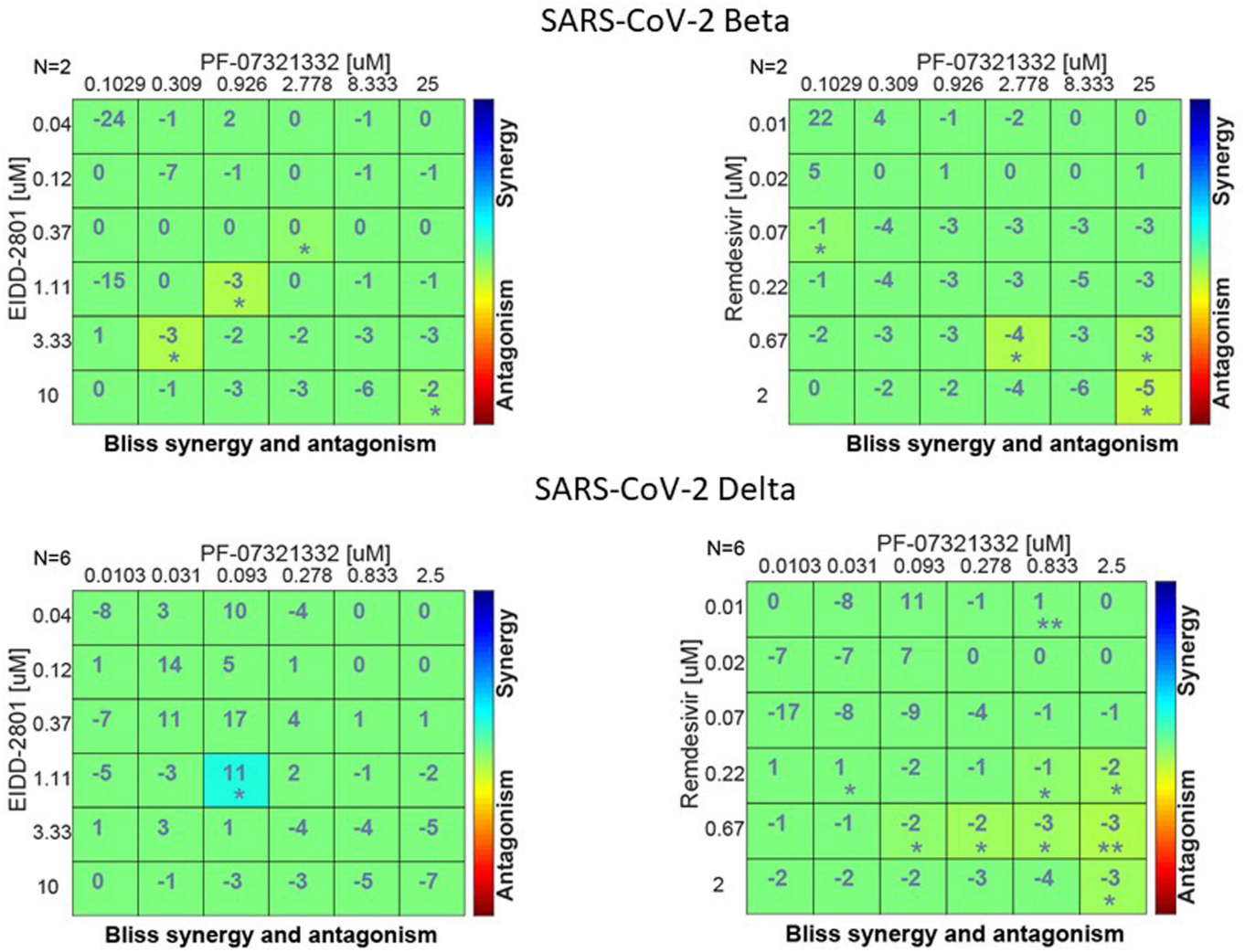

Extended Data Fig. 10 | Combination of molnupiravir or remdesivir with the protease inhibitor PF-07321332 is additive against SARS-CoV-2 (Beta, Delta). BLISS analysis in Calu-3 cells with molnupiravir (EIDD-2801) or remdesivir in combination with PF-07321332 infected with the indicated SARS-CoV-2 variant. Data are presented as mean Excess over BLISS for n = 2 independent biological replicates (SARS-CoV-2 Beta); n = 6 independent biological replicates (SARS-CoV-2 Delta). The statistical significance was determined by a one-sample t-test (* $p < 5x10^{-2}$; ** $p < 10^{-3}$).

nature portfolio

Corresponding author(s): Schultz, Frieman and Cherry

Last updated by author(s): Jan 7, 2022

Reporting Summary

Nature Portfolio wishes to improve the reproducibility of the work that we publish. This form provides structure for consistency and transparency in reporting. For further information on Nature Portfolio policies, see our Editorial Policies and the Editorial Policy Checklist.

Statistics

For all statistical analyses, confirm that the following items are present in the figure legend, table legend, main text, or Methods section.

n/a	Confirmed	
☐	☒	The exact sample size (*n*) for each experimental group/condition, given as a discrete number and unit of measurement
☐	☒	A statement on whether measurements were taken from distinct samples or whether the same sample was measured repeatedly
☐	☒	The statistical test(s) used AND whether they are one- or two-sided *Only common tests should be described solely by name; describe more complex techniques in the Methods section.*
☒	☐	A description of all covariates tested
☒	☐	A description of any assumptions or corrections, such as tests of normality and adjustment for multiple comparisons
☐	☒	A full description of the statistical parameters including central tendency (e.g. means) or other basic estimates (e.g. regression coefficient) AND variation (e.g. standard deviation) or associated estimates of uncertainty (e.g. confidence intervals)
☐	☒	For null hypothesis testing, the test statistic (e.g. *F*, *t*, *r*) with confidence intervals, effect sizes, degrees of freedom and *P* value noted *Give P values as exact values whenever suitable.*
☒	☐	For Bayesian analysis, information on the choice of priors and Markov chain Monte Carlo settings
☒	☐	For hierarchical and complex designs, identification of the appropriate level for tests and full reporting of outcomes
☒	☐	Estimates of effect sizes (e.g. Cohen's *d*, Pearson's *r*), indicating how they were calculated

Our web collection on statistics for biologists contains articles on many of the points above.

Software and code

Policy information about availability of computer code

Data collection	*Provide a description of all commercial, open source and custom code used to collect the data in this study, specifying the version used OR state that no software was used.*
Data analysis	Prism9 and Excel

For manuscripts utilizing custom algorithms or software that are central to the research but not yet described in published literature, software must be made available to editors and reviewers. We strongly encourage code deposition in a community repository (e.g. GitHub). See the Nature Portfolio guidelines for submitting code & software for further information.

Data

Policy information about availability of data

All manuscripts must include a data availability statement. This statement should provide the following information, where applicable:

- Accession codes, unique identifiers, or web links for publicly available datasets
- A description of any restrictions on data availability
- For clinical datasets or third party data, please ensure that the statement adheres to our policy

All data in this paper are presented in the main text and supplementary text. Supplementary Information is available for this paper.

Field-specific reporting

Please select the one below that is the best fit for your research. If you are not sure, read the appropriate sections before making your selection.

☒ Life sciences ☐ Behavioural & social sciences ☐ Ecological, evolutionary & environmental sciences

For a reference copy of the document with all sections, see nature.com/documents/nr-reporting-summary-flat.pdf

Life sciences study design

All studies must disclose on these points even when the disclosure is negative.

Sample size	Use standards in the field for each assay type.
Data exclusions	none
Replication	Every experiment was replicated multiple times as described in the legends.
Randomization	Not applicable, all cell cultures are treated as equal.
Blinding	Performed for histology.

Reporting for specific materials, systems and methods

We require information from authors about some types of materials, experimental systems and methods used in many studies. Here, indicate whether each material, system or method listed is relevant to your study. If you are not sure if a list item applies to your research, read the appropriate section before selecting a response.

Materials & experimental systems

n/a	Involved in the study
☐	☒ Antibodies
☐	☒ Eukaryotic cell lines
☒	☐ Palaeontology and archaeology
☐	☒ Animals and other organisms
☒	☐ Human research participants
☒	☐ Clinical data
☒	☐ Dual use research of concern

Methods

n/a	Involved in the study
☒	☐ ChIP-seq
☒	☐ Flow cytometry
☒	☐ MRI-based neuroimaging

Antibodies

Antibodies used	All listed in methods. Anti J2, Absolute Biosciences.
Validation	All verified by vendors and we verified J2 antibody only detect infected cells.

Eukaryotic cell lines

Policy information about cell lines

Cell line source(s)	All stated in methods. ATCC for all but Huh7.5 (C. Rice), A549 ACE2, (S. Weiss)
Authentication	ATCC , and express lineage specific markers.
Mycoplasma contamination	We perform every 3 months. All cultures were negative.
Commonly misidentified lines (See ICLAC register)	Not used.

Animals and other organisms

Policy information about studies involving animals; ARRIVE guidelines recommended for reporting animal research

Laboratory animals	All specified in methods. 8-10 week old female Balb/C.

Wild animals	None
Field-collected samples	None
Ethics oversight	University of Maryland School of Medicine IACUC

Note that full information on the approval of the study protocol must also be provided in the manuscript.